

# Non-adiabatic particle production scenario in algebraically coupled quintessence field with dark matter fluid

Saddam Hussain\*

*Department of Physics, Indian Institute of Technology Kanpur, UP 208016, India*

(Dated: July 15, 2024)

We investigate the dynamics of an algebraically coupled quintessence field with a dark matter fluid, considering a scenario involving non-adiabatic particle production through the action principle by modifying the interaction Lagrangian. The interaction parameter serves as the source of dark matter particles and entropy production. As particle creation occurs due to the interaction between the field and fluid sectors, the system manifests additional pressure. Our analysis includes studying the system's dynamics by considering an exponential type of interaction corresponding to the field's exponential potential. We assess the system's background dynamics using the dynamical system stability technique and obtain the necessary constraints on the model parameters. We also determine the best-fit values of the model parameters against OHD+Pantheon+ data by adopting a data analysis technique and compare the evidence to  $\Lambda$ CDM. Based on the AIC information criterion, the current model shows strong support; however, the BIC does not show very strong support.

## I. INTRODUCTION

Over the past two decades, observations have shed light on the dynamics of the cosmos at its largest scale, revealing evidence that the expansion of the universe is accelerating [1–9]. One of the most accepted explanations for this late-time cosmic acceleration is the existence of an exotic component known as the cosmological constant ( $\Lambda$ ), which exerts negative pressure. The largest portion of the universe's energy budget consists of the cosmological constant, accounting for about 70%. Additionally, approximately 25% of the energy budget is dominated by a non-relativistic, pressureless fluid commonly referred to as dark matter, with the remaining portion composed of baryonic matter.

Although the  $\Lambda$ CDM model, where CDM refers to cold dark matter, is favored due to its ability to describe most observational evidence, it faces several theoretical shortcomings, including the cosmological constant problem, fine-tuning issues, and the cosmological coincidence problem [10–16]. Additionally, the model exhibits discrepancies between the measured values of the Hubble constant  $H_0$  and the amplitude of matter density  $S_8$  between high and low-redshift data, reaching up to the  $4.2\sigma$  level [17–23]. Consequently, numerous alternatives have been proposed to address these issues, either by modifying the gravitational sector [24–27] or by modifying the matter sector [28–34]. In many instances, scalar fields serve as viable candidates for dark energy (DE) and are often minimally coupled with pressureless dark matter (DM) fluid. However, beyond their gravitational signatures, these enigmatic forms of matter pose puzzles to the scientific community. Consequently, numerous possible scenarios have been intensely investigated, including (i) non-

---

\* [mdsaddamh6@gmail.com](mailto:mdsaddamh6@gmail.com); [msaddam@iitk.ac.in](mailto:msaddam@iitk.ac.in)

gravitational interactions between dark matter and dark energy [35–57] and (ii) non-minimal coupling between matter fields and curvature [58–68].

A recent approach has emerged to investigate the non-gravitational interaction between dark matter (DM) and dark energy (DE) through the variational principle [69–72]. In these studies, dark energy is governed by a scalar field, while the action for the dark matter fluid is modeled using the relativistic fluid action proposed by Brown [73]. This action encompasses the energy density of the fluid  $\rho$ , the particle flux number  $J^\mu$ , and several Lagrange multipliers. Additionally, a non-gravitational interaction term is introduced at the action level, consisting of fluid and field variables, denoted by  $\mathcal{L}_{\text{int}} = -\sqrt{-g}f(n, s, \phi)$ , where  $f$  is an arbitrary interaction function depending on the matter degrees of freedom (fluid number density  $n$ , entropy per particle  $s$ ) and field degrees of freedom  $\phi$ . This type of interaction is called algebraically coupled interaction. It has been shown in ref. [69] that the inclusion of such interaction can manifest an additional interaction energy-momentum tensor in Einstein’s field equations. Consequently, the individual matter components can no longer conserve independently; however, the total energy-momentum tensor of the matter sector remains conserved. In ref. [71], a thorough analysis demonstrated the equivalence of studying the non-gravitational interaction between the dark sector through the variational approach and modifying the matter field equations (the so-called conventional approach) by incorporating a non-vanishing interaction term,  $Q \neq 0$ , i.e.,  $\nabla_\mu T_{\text{DM}}^\mu = -Q = -\nabla_\mu T_\phi^\mu$ , allowing the transportation of energy from dark matter to dark energy or vice versa. However, it has been argued that the latter approach may lead to inconsistencies in defining physical quantities such as the velocity of the individual matter components. At the level of cosmological perturbation, this approach can lead to instability in the early-time epoch [74].

Any models constructed under the interaction function  $f(n, s, \phi)$  are subject to constraints from the fluid Lagrangian, namely the conservation of number density  $\nabla_\mu(nu^\mu) = 0$ , where  $u^\mu$  is the fluid’s four-velocity, and the conservation of entropy density per particle  $\nabla_\mu(snu^\mu) = 0$ . As a result, when evaluating the covariant derivative of the energy-momentum tensor corresponding to the dark matter fluid by decomposing it into components normal and parallel to the fluid’s co-moving velocity  $u^\mu$ , the normal component  $u_\mu \nabla_\nu T_{\text{DM}}^{\mu\nu} = 0$  vanishes, implying that the energy density scales as  $\rho \propto a^{-3}$ , where  $a$  is the scale factor. However, the parallel component does not vanish due to the inclusion of  $\phi$  in the interaction function  $f$ , indicating that the system is non-minimally coupled and evolves adiabatically.

In the past two decades, significant research has been devoted to understanding the dynamics of the very early universe if the particle number density is non-conserved [75–83]. In these scenarios, the background fluid number density is no longer conserved, and a source term is artificially introduced into the number density conservation equation, resulting in the production of creation pressure,  $P_c$ . This matter production phenomenon plays a significant role in describing the reheating phase of the inflationary process [84], and it has also been shown that this effect can significantly contribute to explaining the late-time cosmic acceleration [85, 86].

In this work, we approach the same problem from a new perspective. As stated earlier, a recent approach has been put forth to study non-gravitational interactions from the action principle by introducing an interaction term at the Lagrangian level. To study the matter generation effect from the action principle, we modify the interaction term  $f(n, s, \phi) \rightarrow f(n, s, \phi, \varphi)$ , incorporating a Lagrange multiplier  $\varphi$ . This modification allows the interaction function  $f$  to become the source of particle production. The relativistic fluid action typically consists of several Lagrange multipliers; however, we include one of the fluid scalar fields,  $\varphi$ , which is a gradient of chemical free energy, modifying both the number density ( $\nabla_\mu(nu^\mu) \neq 0$ ) and entropy density per particle ( $\dot{s} \neq 0$ ) conservation equations. This makes the system evolve non-adiabatically in a homogeneous,

isotropic, and spatially flat universe.

In this interaction framework, we evaluated thermodynamic relations, such as the temperature of the dark matter fluid. Since  $f$  becomes the source of particle creation, it also exerts creation pressure. Hydrodynamically, this creation pressure can be interpreted as viscous pressure, rendering the background fluid an imperfect fluid. We conducted an in-depth analysis of the background dynamics of this non-minimal coupling scenario using the dynamical system stability technique [87–91], considering an exponential type of interaction  $f \propto \rho^\beta e^{\delta\kappa\phi+\gamma\varphi}$  corresponding to the exponential potential for the quintessence field. The choice of exponential interaction function is purely phenomenological, ensuring non-zero effects during both non-accelerating and accelerating regimes. We studied the system's dynamics corresponding to the models  $f \propto \rho^2$  and  $f \propto \rho^{-1}$ . The system yields a late-time accelerating stable phase followed by an attractor matter-dominated phase. Furthermore, we constrain the model parameter space by adopting the data analysis technique corresponding to the combined 43 Hubble and 1701 Pantheon+ data points.

The paper is organized as follows: In Sec. II, we set up the action for the algebraically coupled field-fluid system and obtain the governing background equations. In Sec. III, we present brief thermodynamic relations corresponding to the fluid component. A detailed picture of the conservation of the energy-momentum tensor is presented in Sec. IV. The stability of the dynamical system is discussed in Sec. V. In Sec. VI, the model parameters are constrained using data analysis. Finally, a brief conclusion is outlined in Sec. VII.

## II. ACTION FOR THE ALGEBRAIC INTERACTION

The action describing the algebraically (non-minimally) coupled field-fluid scenario for the modified interaction term is given by:

$$S = \int_{\Omega} d^4x \sqrt{-g} \frac{R}{2\kappa^2} - \sqrt{-g} \rho(n, s) + J^\mu (\varphi_{,\mu} + s\theta_{,\mu} + \alpha_A \beta_{,\mu}^A) - \sqrt{-g} \mathcal{L}_\phi(\phi, \partial_\mu \phi) - \alpha_1 \sqrt{-g} f(n, s, \phi, \varphi), \quad (2.1)$$

where,

$$J^\mu = \sqrt{-g} n u^\mu, \quad |J| = \sqrt{-g_{\mu\nu} J^\mu J^\nu}, \quad n = \frac{|J|}{\sqrt{-g}}, \quad u^\mu u_\mu = -1. \quad (2.2)$$

In this action, the first term corresponds to the Einstein-Hilbert action, where  $g$  denotes the determinant of the metric tensor  $g^{\mu\nu}$ ,  $R$  represents the Ricci scalar, and  $\kappa^2 = 8\pi G$ . The second and third terms together represent the action for a relativistic fluid, where the energy density of the dark matter fluid is denoted as  $\rho$ , depending on the fluid number density  $n$  and the entropy density per particle  $s$ . The other term contains the particle flux density  $J^\mu$  and Lagrange multipliers  $\varphi$ ,  $\theta$ ,  $\alpha^A$ ,  $\beta_A$ . Note that Greek indices range from 0 to 3, and  $A$  runs from 1 to 3. It's important to distinguish between  $\alpha_1$  and  $\alpha^A$  as they are distinct quantities unless specified. The commas followed by Greek indices indicate covariant derivatives. The field action is given by:

$$\mathcal{L}_\phi = \frac{1}{2} \partial_\mu \phi \partial^\mu \phi + V(\phi). \quad (2.3)$$

Here, the Lagrangian represents a standard quintessence field with the potential  $V(\phi)$ . The remaining term in the action corresponds to the interaction parameter  $f$ , which depends on fluid and field parameters, while  $\alpha_1$  is a constant parameter. Taking the variation of the action Eq. (2.1)

with respect to the metric  $g^{\mu\nu}$  yields the Einstein field equation:

$$R_{\mu\nu} - \frac{1}{2}Rg_{\mu\nu} = \kappa^2 \left( T_{\mu\nu}^M + T_{\mu\nu}^\phi + T_{\mu\nu}^{\text{int}} \right). \quad (2.4)$$

Here, the stress tensor of the matter components is defined as  $T_{\mu\nu} \equiv \frac{-2}{\sqrt{-g}} \frac{\delta S}{\delta g^{\mu\nu}}$ . The energy-momentum tensor corresponding to the relativistic fluid is:

$$T_M^{\mu\nu} = \rho u^\mu u^\nu + \left( n \frac{\partial \rho}{\partial n} - \rho \right) (u^\mu u^\nu + g^{\mu\nu}). \quad (2.5)$$

Similarly, corresponding to the interaction part:

$$T_{\text{int}}^{\mu\nu} = \alpha_1 f u^\mu u^\nu + \alpha_1 \left( n \frac{\partial f}{\partial n} - f \right) (u^\mu u^\nu + g^{\mu\nu}). \quad (2.6)$$

The field's stress tensor becomes:

$$T_\phi^{\mu\nu} = -g^{\mu\nu} \left( \frac{1}{2} \partial_\alpha \phi \partial^\alpha \phi + V(\phi) \right) + \partial^\mu \phi \partial^\nu \phi. \quad (2.7)$$

To evaluate the energy density and corresponding pressure of these matter components, we compare with the stress tensor for the perfect fluid  $T^{\mu\nu} = \rho u^\mu u^\nu + P(g^{\mu\nu} + u^\mu u^\nu)$ . Hence, the energy density and pressure of the fluid become:

$$\rho_M = \rho, \quad P_M = \left( n \frac{\partial \rho}{\partial n} - \rho \right). \quad (2.8)$$

The energy density and pressure corresponding to the algebraic interaction are:

$$\rho_{\text{int}} = \alpha_1 f, \quad P_{\text{int}} = \alpha_1 \left( n \frac{\partial f}{\partial n} - f \right). \quad (2.9)$$

The field energy density and pressure become:

$$\rho_\phi = \frac{1}{2} \dot{\phi}^2 + V(\phi), \quad P_\phi = \frac{1}{2} \dot{\phi}^2 - V(\phi). \quad (2.10)$$

In the flat FLRW metric  $ds^2 = -dt^2 + a(t)^2 d\vec{x}^2$ , the Friedmann equations become:

$$3H^2 = \kappa^2 (\rho_M + \rho_\phi + \rho_{\text{int}}), \quad (2.11)$$

$$2\dot{H} + 3H^2 = -\kappa^2 (P_M + P_\phi + P_{\text{int}}). \quad (2.12)$$

Upon taking the variation of the action with respect to  $\phi$ , the field equation becomes:

$$\ddot{\phi} + 3H\dot{\phi} + \frac{dV(\phi)}{d\phi} + \alpha_1 \frac{\partial f}{\partial \phi} = 0. \quad (2.13)$$

### III. THERMODYNAMIC RELATIONS

In this section, we will examine the thermodynamic aspect of the fluid in light of interaction. Upon varying the action with respect to the fluid variables, the corresponding equations of motion become:

$$J^\mu : \quad u_\mu \left( \frac{\partial \rho}{\partial n} + \alpha_1 \frac{\partial f}{\partial n} \right) + \varphi_{,\mu} + s\theta_{,\mu} + \beta_A \alpha_{,\mu}^A = 0, \quad (3.1)$$

$$s : \quad - \left( \frac{\partial \rho}{\partial s} + \alpha_1 \frac{\partial f}{\partial s} \right) + nu^\mu \theta_{,\mu} = 0, \quad (3.2)$$

$$\varphi : \quad \nabla_\mu (nu^\mu) + \alpha_1 \frac{\partial f}{\partial \varphi} = 0, \quad (3.3)$$

$$\theta : \quad (sJ^\mu)_{,\mu} = 0, \quad (3.4)$$

$$\beta_A : \quad J^\mu \alpha_{,\mu}^A = 0, \quad (3.5)$$

$$\alpha^A : \quad (\beta_A J^\mu)_{,\mu} = 0. \quad (3.6)$$

To understand the physical meaning of some of the Lagrange multipliers, consider the case where the interaction parameter is switched off, i.e.,  $\alpha_1 = 0$ . In this scenario, Eqs. (3.3) and (3.4) yield conserved fluid number density,  $\nabla_\mu (nu^\mu) = 0$ , and conserved entropy density,  $\dot{s} = 0$ , in the flat FLRW metric. From Eq. (3.2), the temperature of the fluid is defined as  $T \equiv \frac{1}{n} \frac{\partial \rho}{\partial s} \Big|_n$ , the Lagrange multiplier  $\theta$  becomes the potential for the temperature. Similarly, it can be shown using Eqs. (3.1), (3.2), and (3.5) that  $\varphi$  is the potential for chemical free energy  $F \equiv \mu - Ts = \varphi_{,\mu} u^\mu$ , where  $\mu = \frac{\partial \rho}{\partial n}$  is the chemical potential.

Due to the modifications in the interaction parameter, which now includes the Lagrange parameter  $\varphi$ , the number density of the fluid from Eq. (3.3) is no longer conserved, and the interaction parameter  $f$  acts as a source of fluid particle production. In the flat FLRW background metric, this equation reads as:

$$\dot{n} + 3nH = -\alpha_1 \frac{\partial f}{\partial \varphi}. \quad (3.7)$$

Here, we have included the Lagrange multiplier  $\varphi$  in the interaction function, but one may also add  $\theta$  dependence, resulting in the interaction function  $f(n, s, \phi, \varphi, \theta)$ . The inclusion of  $\theta$  only modifies Eq. (3.4), and the corresponding equation of motion becomes:

$$\nabla_\mu (snu^\mu) = -\alpha_1 \frac{\partial f}{\partial \theta}. \quad (3.8)$$

Now, using Eq. (3.7), the entropy evolution equation becomes:

$$\dot{s} = \frac{\alpha_1}{n} \left( s \frac{\partial f}{\partial \varphi} - \frac{\partial f}{\partial \theta} \right). \quad (3.9)$$

It is important to note that if the interaction function only depends on the temperature potential  $\theta$ , the fluid evolves non-adiabatically while the particle number density remains conserved. However, the inclusion of  $\varphi$  in the interaction function can simultaneously generate matter and entropy production in the background fluid. If the interaction function  $f$  depends on both Lagrange multipliers, an interesting phenomenon may occur. The derivatives inside the parenthesis in the

above equation take alternate signs, and it is possible for certain model choices that:

$$\left( s \frac{\partial f}{\partial \varphi} - \frac{\partial f}{\partial \theta} \right) = 0. \quad (3.10)$$

This scenario indicates the adiabatic matter production mechanism. However, for simplicity, we proceed with the interaction function as defined in Eq. (2.1). The corresponding contribution to entropy becomes:

$$\dot{s} = \frac{s}{n} \alpha_1 \frac{\partial f}{\partial \varphi}. \quad (3.11)$$

Hence, the dependence of  $\varphi$  in the interaction function may increase or decrease the fluid particle density, resulting in a change in entropy. Consequently, the evolution of the fluid sector becomes non-adiabatic. As the interaction parameter induces changes in number density and entropy, the corresponding change in energy density of the fluid sector can be explored using the thermodynamic relation:

$$d(\rho V) = dQ - PdV. \quad (3.12)$$

Here,  $dQ$  denotes the heat received by the fluid sector during time  $dt$ , and  $V = a^3$  signifies the comoving volume. For the closed system, the above relation can be re-expressed as:

$$d(\rho/n) = Tds - Pd(1/n). \quad (3.13)$$

Here,  $dq = dQ/N$ ,  $n = N/V$ ,  $s = S/N$ , and  $T = \frac{1}{n} \left. \frac{\partial \rho}{\partial s} \right|_n$  is the temperature of the fluid [76]. As the particle production takes place, the system can absorb heat. The above relation can then be extended to the open system as:

$$d(\rho V) = TV(d(sn) - sdn) - PdV + \frac{\rho + P}{n} d(nV). \quad (3.14)$$

On differentiating both sides with respect to time  $t$ , we obtain:

$$\dot{\rho} + 3H(\rho + P) = Ts\alpha_1 \frac{\partial f}{\partial \varphi} - \alpha_1 \frac{\rho + P}{n} \frac{\partial f}{\partial \varphi}. \quad (3.15)$$

From this, we can express the creation pressure or non-minimally induced pressure  $P_c$  as:

$$P_c = \frac{1}{3H} \left( \frac{\rho + P}{n} - \frac{s}{n} \frac{\partial \rho}{\partial s} \right) \alpha_1 \frac{\partial f}{\partial \varphi}. \quad (3.16)$$

Therefore, as the fluid's particle number density changes, the system can exhibit an additional pressure known as creation pressure. The density evolution can be rewritten as:

$$\dot{\rho} + 3H(\rho + P + P_c) = 0. \quad (3.17)$$

From Eq. (3.7) and Eq. (3.11), it is clear that if  $\alpha_1 \frac{\partial f}{\partial \varphi} < 0$ , the interaction contributes to an increment in the number density of the fluid particles. As a consequence, the change in entropy corresponding to the fluid sector decreases. Although the entropy of the matter sector decreases, it's important to note that the entropy of the system as a whole may not decrease. Hence, the second law of thermodynamics for the entire system remains intact.

Using the above equation, the evolution of the temperature  $T$  of the fluid can be determined. We utilize the total derivative of energy density as:

$$d\rho(n, T) = \left(\frac{\partial\rho}{\partial n}\right)_T dn + \left(\frac{\partial\rho}{\partial T}\right)_n dT, \quad (3.18)$$

After taking the time derivative and using equations Eq. (3.17) and Eq. (3.7), we obtain:

$$\dot{T} = \frac{1}{(\partial\rho/\partial T)_n} \left( -3H(\rho + P + P_c) - \left(\frac{\partial\rho}{\partial n}\right)_T \dot{n} \right). \quad (3.19)$$

To evaluate  $\left(\frac{\partial\rho}{\partial n}\right)_T$ , we use the thermodynamic relation:

$$ds = \frac{1}{nT} d\rho - \frac{\rho + P}{n^2 T} dn, \quad (3.20)$$

and using the partial derivative property, we obtain:

$$\left(\frac{\partial s}{\partial n}\right)_T = \frac{1}{nT} \left( \left(\frac{\partial\rho}{\partial n}\right)_T - \frac{\rho + P}{n} \right), \quad \left(\frac{\partial s}{\partial T}\right)_n = \frac{1}{nT} \left(\frac{\partial\rho}{\partial T}\right)_n. \quad (3.21)$$

Further using the property  $\frac{\partial^2 s}{\partial T \partial n} = \frac{\partial^2 s}{\partial n \partial T}$ , we get:

$$h = \rho + P = n \left(\frac{\partial\rho}{\partial n}\right)_T + T \left(\frac{\partial P}{\partial T}\right)_n. \quad (3.22)$$

Here,  $h$  is the enthalpy per unit volume. Inserting this relation into  $\dot{T}$  and using  $\frac{(\partial P/\partial T)_n}{(\partial\rho/\partial T)_n} \equiv (\partial P/\partial\rho)_n$ , we finally obtain:

$$\dot{T}/T = \frac{s\alpha_1 \partial f/\partial\varphi}{(\partial\rho/\partial T)_n} + \frac{\dot{n}}{n} \left(\frac{\partial P}{\partial\rho}\right)_n. \quad (3.23)$$

Using Eq. (3.11), this relation is similar to the one that has been obtained in ref. [92]. The first term on the right-hand side shows the contribution from the non-conserved entropy of the fluid. To find the temperature evolution, we choose the model corresponding to the pressureless non-relativistic fluid. The energy density of the non-relativistic ideal gas ( $k_B = 1$ ) is:

$$\rho = Mn + \frac{3}{2}nT, \quad (3.24)$$

where  $M$  is the mass of gas particles. Corresponding to this ideal gas model, the pressure,  $P = n(\partial\rho/\partial n) - \rho = 0$ , vanishes. Using this relation, the temperature relation simplifies to:

$$\frac{\dot{T}}{T} = \frac{2\dot{s}}{3}. \quad (3.25)$$

This gives the variation of temperature with entropy irrespective of any form of interaction param-

eter  $f$ . Hence the entropy becomes:

$$s = s_0 + \frac{3}{2} \ln(T/T_0). \quad (3.26)$$

Here, the parameters with subscript 0 are integration constants representing the present value of the respective parameters.

#### IV. CONSERVATION OF ENERGY MOMENTUM TENSOR

In the preceding section, we explored the thermodynamic behavior of the fluid sector, employing thermodynamic relations to determine the corresponding evolution of fluid density. In this section, we delve into evaluating the covariant derivative of the stress tensor of the entire system to investigate the transportation of energy flow between the fluid and field sectors. To do so, we first redefine the matter stress tensor as:

$$T_A^{\mu\nu} = (\rho + \alpha_1 f) u^\mu u^\nu + \left( n \frac{\partial \rho}{\partial n} - \rho + \alpha_1 n \frac{\partial f}{\partial n} - \alpha_1 f \right) (u^\mu u^\nu + g^{\mu\nu}). \quad (4.1)$$

With this redefinition, the Einstein tensor becomes  $G_{\mu\nu} = \kappa^2 (T_{\mu\nu}^A + T_{\mu\nu}^\phi)$ <sup>1</sup>. Upon taking the covariant derivative of the stress tensor, we obtain:

$$\nabla_\mu T_A^{\mu 0} = \dot{\rho} + \alpha_1 \dot{f} + 3H(\rho + \alpha_1 f + P_M + P_{\text{int}}) = Q^0. \quad (4.2)$$

Utilizing Eq. (3.7) and Eq. (3.11), we can express:

$$\nabla_\mu T_A^{\mu 0} = \dot{\rho} + 3H(\rho + P_M) - \alpha_1^2 \frac{\partial f}{\partial \varphi} \frac{\partial f}{\partial n} + \alpha_1 \dot{\phi} \frac{\partial f}{\partial \phi} + \alpha_1^2 \frac{\partial f}{\partial s} \left( \frac{s}{n} \frac{\partial f}{\partial \varphi} \right) + \alpha_1 \dot{\phi} \frac{\partial f}{\partial \varphi} = Q^0. \quad (4.3)$$

To eliminate  $\dot{\phi}$  from the above equation, we contract Eq. (3.1) with  $J^\mu$  and then use Eq. (3.5), we get:

$$\frac{\partial \rho}{\partial n} - s\dot{\theta} + \alpha_1 \frac{\partial f}{\partial n} = \dot{\phi}, \quad (4.4)$$

which, when inserted into the above equation, yields:

$$\nabla_\mu T_A^{\mu 0} = \dot{\rho} + 3H(\rho + P_M) + \alpha_1 \dot{\phi} \frac{\partial f}{\partial \phi} + \alpha_1 \frac{\partial \rho}{\partial n} \frac{\partial f}{\partial \varphi} + \alpha_1^2 \frac{\partial f}{\partial s} \left( \frac{s}{n} \frac{\partial f}{\partial \varphi} \right) - s\dot{\theta} \frac{\partial f}{\partial \varphi}, \quad (4.5)$$

The time derivative of the temperature gradient  $\dot{\theta}$  can be eliminated by using Eq. (3.2), resulting in:

$$\nabla_\mu T_A^{\mu 0} = \dot{\rho} + 3H(\rho + P_M) + \alpha_1 \dot{\phi} \frac{\partial f}{\partial \phi} + \alpha_1 \frac{\partial \rho}{\partial n} \frac{\partial f}{\partial \varphi} - \alpha_1 \frac{s}{n} \frac{\partial f}{\partial \varphi} \frac{\partial \rho}{\partial s}. \quad (4.6)$$

Using the definition of the pressure of the fluid  $P_M + \rho = n \frac{\partial \rho}{\partial n}$  and comparing this with Eq. (3.15), we obtain:

$$\nabla_\mu T_A^{\mu 0} = \dot{\rho} + 3H(\rho + P_M + P_c) + \alpha_1 \dot{\phi} \frac{\partial f}{\partial \phi} = Q^0, \quad (4.7)$$

<sup>1</sup> Here  $A$  denotes a label.



where  $P_c = \frac{1}{3H} \left( \frac{\rho + P_M}{n} \alpha_1 \frac{\partial f}{\partial \varphi} - \alpha_1 \frac{s}{n} \frac{\partial f}{\partial \varphi} \frac{\partial \rho}{\partial s} \right)$ . Considering Eq. (3.15), the covariant derivative of the fluid sector yields:

$$\nabla_\mu T_A^{\mu 0} = \alpha_1 \dot{\phi} \frac{\partial f}{\partial \phi} = Q^0. \quad (4.8)$$

The covariant derivative of the field sector can be determined using Eq. (2.13) as:

$$\nabla_\mu T_\phi^{\mu 0} = -\alpha_1 \frac{\partial f}{\partial \phi} \dot{\phi} = -Q^0. \quad (4.9)$$

This exercise demonstrates that the total energy density of the system remains conserved, and both sectors exchange energy through the interaction term:

$$Q^0 = \alpha_1 \frac{\partial f}{\partial \phi} \dot{\phi}. \quad (4.10)$$

## V. BACKGROUND DYNAMICS

In this section, we will conduct a stability analysis of the system using the standardized linearization technique. We observed that the interaction function alters not only the field's equation of motion but also the fluid's equation of motion. As the non-minimal coupling parameter  $f$  acts as a source of particle creation and entropy generation, the system transitions to a non-adiabatic state. Hence, evaluating the stability of the system becomes crucial for this complex model.

The dynamical system stability technique provides a mathematical framework to study the physical properties of these non-linear models and constrain the parameter space based on the stability of the critical points. This approach is particularly useful when the number of parameters is comparatively large, making it important to determine stability at the background level. To elucidate the background evolution of the system, we define a set of dimensionless dynamical variables as:

$$x = \frac{\kappa \dot{\phi}}{\sqrt{6}H}, \quad y = \frac{\kappa \sqrt{V}}{\sqrt{3}H}, \quad z = \frac{\kappa^2 f}{3H^2}, \quad \Omega_\phi = \frac{\kappa^2 \rho_\phi}{3H^2}, \quad \Omega_M = \frac{\kappa^2 \rho}{3H^2}. \quad (5.1)$$

Expressing the first Friedmann equation in dynamical variables puts constraint on the fluid fractional energy density as:

$$\Omega_M = 1 - x^2 - y^2 - \alpha_1 z, \quad (5.2)$$

and the effective equation of state (EoS) corresponding to the composite system becomes:

$$\omega_{\text{eff}} = \frac{P_{\text{tot}}}{\rho_{\text{tot}}} = x^2 - y^2 + \alpha_1 (\beta - 1) z. \quad (5.3)$$

Here,  $\beta$  represents the model parameter chosen for the interaction function  $f$  as shown in Eq. (5.5). Based on the definition of the dynamical variables, the ranges of the variables are as follows:

$$-\infty < x < +\infty, \quad 0 \leq y < \infty, \quad -\infty < z < +\infty, \quad 1 > \Omega_M > 0, \quad 1 > \Omega_\phi > 0. \quad (5.4)$$

As the model is non-linear and complex, obtaining an analytical solution for stability analysis with any general form of  $f$  is a cumbersome task. Although the phenomenon of particle production is not new, and the quantum theory for these dark components is still unknown, it is crucial to explore all

possible forms of  $f$ . However, within the framework of dynamical system analysis, it is preferable to choose the model such that the phase space corresponding to the system remains constrained to 3D. As the number of dynamical variables increases, the analysis becomes increasingly difficult. Keeping this in mind, we choose the exponential type of interaction as considered in [69]:

$$f = M^{4-4\beta} \rho^\beta e^{(\delta\kappa\phi + \gamma\varphi)}. \quad (5.5)$$

Here, we also take an exponential form corresponding to the fluid variable  $\varphi$  to simplify the mathematical complexity. We choose an exponential type potential corresponding to the quintessence field, as this form of potential has been widely studied. The quintessence field with an exponential potential exhibits an attractor scaling solution during the matter-dominated epoch and stabilizes in the late-time epoch as the field exhibits a tracking solution. The potential is given by:

$$V(\phi) = V_0 e^{\lambda\kappa\phi}. \quad (5.6)$$

Now, as the interaction function depends on several field and fluid variables, it is important to evaluate  $\dot{z}$  corresponding to the interaction function Eq. (5.5):

$$\dot{z} = \frac{\kappa^2}{3H^2} (-3H\beta f + \delta\kappa f \dot{\phi} + \gamma f (\rho/n - sT)) - z \frac{\dot{H}}{H}. \quad (5.7)$$

Here, we see that the derivative yields field variables  $\dot{\phi}$  which can be re-expressed in terms of predefined dynamical variables. However, the derivative also yields certain thermodynamic variables which cannot be expressed in terms of predefined variables. To address this, we need to define some additional variables corresponding to  $(n, s, T)$ , as these quantities are time-dependent. The derivative has been evaluated using  $T = \frac{1}{n} \frac{\partial \rho}{\partial s}$ , Eq. (4.4), and  $\dot{\theta} = T + \alpha_1 \frac{1}{n} \frac{\partial f}{\partial s}$ . Hence, the additional dimensionless dynamical variables are:

$$\chi = \frac{\kappa^2 n}{3H}, \quad \xi = T/H, \quad s = s. \quad (5.8)$$

We choose the variables corresponding to the number density  $n$ , temperature  $T$  of the fluid, and entropy  $s$ . With these definitions, the thermodynamic variables are constrained within the following ranges:

$$\chi > 0, \quad \xi > 0, \quad s \geq 0. \quad (5.9)$$

With these new variables, the total number of independent dynamical variables becomes 6, i.e.,  $(x, y, z, \chi, \xi, s)$ . As a result, the phase space of the system extends to 6-D. Therefore, for the exponential type of interaction, the phase space of the system cannot be constrained to 3-D. In addition to the extended phase space dimension, this 6-D space is unconstrained, as some of the dynamical variables can take any values. However, in the present study, our primary goal is to explore the stability of the model during the matter-dominated and current epochs of the universe. It is possible that the study of the very early phase of the universe may result in pathological solutions corresponding to these unconstrained variables. In such cases, one must adopt the Poincare compactification for those dynamical variables [93].

In terms of the additionally defined variables, the aforementioned dynamical equation for  $z'$  becomes:

$$z' = \frac{\dot{z}}{H} = -3\beta z + \delta z x \sqrt{6} + \gamma z (\Omega_M / \chi - s \xi) + \frac{3}{2} z (1 + x^2 - y^2 + (\beta - 1) z \alpha_1). \quad (5.10)$$

By expressing  $(\dot{\phi}, \dot{n}, \dot{s}, \text{ and } \dot{T})$  in terms of the dynamical variables  $(x, y, z, \chi, \xi, s)$ , we can now write the complete set of autonomous equations governing the system. The autonomous system of equations that describes the dynamics of the entire system are:

$$x' = -3x - \frac{3\lambda y^2}{\sqrt{6}} - \frac{\delta\alpha_1 3z}{\sqrt{6}} + \frac{3}{2}x(1 + x^2 - y^2 + (\beta - 1)z\alpha_1), \quad (5.11)$$

$$y' = \frac{\sqrt{6}yx\lambda}{2} + \frac{3}{2}y(1 + x^2 - y^2 + (\beta - 1)z\alpha_1), \quad (5.12)$$

$$z' = -3\beta z + \delta z x \sqrt{6} + \gamma z (\Omega_M / \chi - s \xi) + \frac{3}{2}z(1 + x^2 - y^2 + (\beta - 1)z\alpha_1), \quad (5.13)$$

$$\chi' = -\alpha_1 \gamma z - 3\chi + \frac{3}{2}\chi(1 + x^2 - y^2 + (\beta - 1)z\alpha_1), \quad (5.14)$$

$$\xi' = \frac{2\xi s \alpha_1 z \gamma}{3\chi} + \frac{3}{2}\xi(1 + x^2 - y^2 + (\beta - 1)z\alpha_1), \quad (5.15)$$

$$s' = \frac{s \alpha_1 z \gamma}{\chi}. \quad (5.16)$$

Here, we obtained the dynamics corresponding to the temperature parameter using Eq. (3.23), where we evaluated  $(\partial\rho/\partial T)_n$  by considering the ideal gas model given in Eq. (3.24). Due to the non-adiabatic particle production mechanism, the degrees of freedom to describe the dynamics of the system increase to 6-dimensions. It's important to note that although we have assumed dark matter to behave as an ideal gas, with its energy density given by Eq. (3.24), this alone cannot provide a constraint on either  $\chi$  or  $\xi$ . An additional variable is needed to capture the dynamics of  $H$  to close the autonomous system of equations. As a result, the dimension of the phase space remains 6-D. Hence, keeping  $\chi$  and  $\xi$  as dynamical variables reduces the complexity of obtaining the critical points as no logarithmic function will appear. The autonomous equations in  $(y', z', \xi', s')$  are invariant under the transformations  $(y \mapsto -y, z \mapsto -z, \xi \mapsto -\xi, s \mapsto -s)$ , presenting an invariant sub-manifold at  $(y = z = \xi = s = 0)$ . This implies that no trajectory originating in  $(y, z, \xi, s \geq 0)$  can cross the  $(y = z = \xi = s = 0)$  plane.

In order to obtain the physical properties of the model and constrain the model parameters, we determine the critical points by equating the right-hand side of the autonomous equations to zero. Here, we can see that the differential equation corresponding to  $s'$  imposes stringent constraints on  $z$ , as the critical points can only be obtained when either  $s = 0$  or  $z = 0$ . In addition, we observe that both  $s'$  and  $z'$  diverge for  $\chi \rightarrow 0$ . This indicates that either  $n \rightarrow 0$  or  $H \gg 1$ . As  $n \rightarrow 0$  may represent the future epoch of the universe, whereas  $H \gg 1$  indicates the past epoch of the universe. Therefore, to regularize the system corresponding to these critical points, we redefine the time variable as suggested in [88]:

$$dN \rightarrow \chi d\tilde{N}. \quad (5.17)$$

Since the number of e-folds  $N$  is a monotonically increasing function, the newly defined variable  $\tilde{N}$  also becomes a monotonically increasing function, given that the dynamical variable  $\chi > 0$  is strictly assumed to be positive in this context. By employing this redefinition, we ensure the regularity of the system and facilitate the stability analysis of the model.

As Eq. (5.16) yields the critical point when  $s = 0$  or  $z = 0$ , we consider the case where  $(z = \frac{\kappa^2 f}{3H^2} = 0)$  and  $s \neq 0$  as one of the coordinates of the critical points. This indicates that either  $f$  vanishes or  $H \gg 1$ . If  $f \rightarrow 0$ , the corresponding particle production freezes, as indicated by

Eq. (3.7). Consequently,  $\dot{s}$  vanishes, and the system evolves adiabatically with conserved number density. This particular case may be realized in the current or late-time epoch of the universe, where the rate of particle production may decrease due to expansion.

On the other hand, if  $s = 0$  serves as one of the coordinates of the critical point and  $z \neq 0$ , Eq. (3.7) and Eq. (3.11) imply that particle production takes place adiabatically as  $\dot{s}$  vanishes. The temperature evolution from Eq. (3.25), corresponding to the dark matter fluid (considered as a pressureless ideal gas), freezes. Hence, the production of dark matter particles may not alter the temperature of the universe. This scenario signifies the matter and late-time state of the universe.

Now we shall determine the critical points corresponding to the autonomous equations, Eq. (5.11)–Eq. (5.16), for  $s = 0$ . The summary of the critical points is tabulated in Tab. [I] for the redefined time variable. We then tabulate the physical behavior based on the effective equation of state (EoS)  $\omega_{\text{eff}}$  and fractional energy densities in Tab. [II], where we outline the existence conditions based on the constraints on dynamical variables Eq. (5.9).

We discuss the stability of the critical points by utilizing the standard linearization technique. To do this, we expand the autonomous system of equations, Eq. (5.11)–Eq. (5.16), using the Taylor series expansion up to the first order at the critical points. Subsequently, a Jacobian matrix  $J_{ij} = \left. \frac{dx'_i}{dx_j} \right|_{(x_{i*})}$  can be constructed. The real parts of the eigenvalues of this matrix indicate the stability of the critical point. If the real parts of the eigenvalues are all positive (negative), the point becomes an unstable (stable) point. For alternate signs of the real parts, the point becomes a saddle point. If any real part vanishes, the linearization technique becomes invalid for determining the stability of that critical point. In such cases, one must apply the center manifold theorem or numerical analysis to determine the asymptotic behavior of the fixed point.

The model yields 12 critical points summarized in Tab. [I]. Among these critical points, a few have vanishing  $z$ , resulting in the vanishing of some thermodynamic variables. These critical points represent the case where the quintessence field is minimally coupled with the dark matter fluid. The critical points corresponding to this scenario are  $P_{4\mp}$ ,  $P_6$ ,  $P_7$ , and  $P_9$ . The discussion of these critical points can be found extensively in the literature, as substantial investigation has been done in the past on the quintessence field assuming an exponential type potential. Interested readers may refer to [94] and references therein. The behavior of the critical points is discussed as follows:

- **Point  $P_{1\pm}$ :** At these points, the potential parameter  $y$  and the temperature parameter  $\xi$  vanish, while the kinetic part of the field  $x$  is non-zero. The temperature parameter vanishes when  $H \gg 1$ , indicating the early epoch of the universe. We are avoiding the condition when temperature  $T \rightarrow 0$  as it may indicate the future epoch of the universe. This is because the potential of the field vanishes, making the field less suitable for driving late-time cosmic acceleration. The fractional energy densities of the field and fluid at these points are summarized in Tab. [II]. The points yield finite energy density for both matter components and exhibits an accelerating solution with an effective equation of state  $\omega_{\text{eff}} = -1$ . If this point considers to indicate the early-time accelerating scenario, then the field fractional density must dominate over the fluid energy density at that epoch, i.e.,  $\Omega_\phi \gg \Omega_M$ .

If we impose the constraints  $0.9 < \Omega_\phi < 1$  and  $0 < \Omega_M < 0.1$  on both critical points, the corresponding constraints on the model parameters  $\beta$  and  $\delta$  for the points  $P_{1\mp}$  become:

$$\begin{aligned}
 P_{1-}: \quad & 0.816\sqrt{\delta^2 + 1.0} \leq \beta < 0.472\sqrt{3.0\delta^2 + 5.0} + 0.944, \quad (\delta > 24.50, \delta < -24.50), \\
 P_{1+}: \quad & 1.0 - 0.817\sqrt{\delta^2} < \beta < 1.0 - 0.577\sqrt{2.0\delta^2 + 3.0}, \quad (\delta > 23.23, \delta < -23.24).
 \end{aligned}$$

TABLE I: The critical points corresponding to autonomous system of equations Eq. (5.11)–Eq. (5.16).

$s_* = 0$					
Points	$x_*$	$y_*$	$z_*$	$\chi_*$	$\xi_*$
$P_{1\mp}$	$\frac{-\sqrt{6+\sqrt{6}\beta\mp r}}{2\delta}$ <sup>a</sup>	0	$\frac{3-3\beta\pm p}{\alpha_1\delta^2}$	$\frac{\gamma(-3+3\beta\mp p)}{3\delta^2}$	0
$P_{2\mp}$	$\frac{-3+3\beta\mp p}{\sqrt{6}\delta}$ <sup>b</sup>	0	$\frac{3-3\beta\pm p}{\alpha_1\delta^2}$	$\frac{\gamma(-3+3\beta\mp p)}{3\delta^2}$	Any
$P_3$	0	$\frac{\sqrt{\delta}}{\sqrt{(\beta-1)\lambda+\delta}}$	$-\frac{\lambda}{\alpha_1((\beta-1)\lambda+\delta)}$	$\frac{\gamma\lambda}{3((\beta-1)\lambda+\delta)}$	Any
$P_{4\mp}$	$\mp 1$	0	0	0	0
$P_5$	$\frac{\sqrt{\frac{3}{2}}(\beta-1)}{\delta}$	$\frac{\sqrt{\frac{3}{2}}}{\lambda}$	$\frac{-3\beta-\delta\lambda+3}{\alpha_1\delta^2}$	$\frac{2\gamma(3\beta+\delta\lambda-3)}{3\delta((\beta-1)\lambda+2\delta)}$	0
$P_6$	$-\frac{\sqrt{\frac{3}{2}}}{\lambda}$	$\frac{\sqrt{\frac{3}{2}}}{\lambda}$	0	0	0
$P_7$	$-\frac{\lambda}{\sqrt{6}}$	$\sqrt{1-\frac{\lambda^2}{6}}$	0	0	0
$P_8$	Any	Any	$-\frac{x^2+y^2-1}{\alpha_1}$	0	Any
$P_9$	Any	Any	0	0	Any

$$^a r = \sqrt{6\beta^2 - 12\beta - 4\delta^2 + 6}$$

$$^b p = \sqrt{9\beta^2 - 18\beta - 6\delta^2 + 9}$$

From this range, it can be concluded that if the model is to describe an early accelerating phenomenon, the corresponding model parameters need to be fine-tuned. When selecting these parameter ranges, it is possible that the other critical points may not exist. Upon evaluating the stability within these ranges, the point consistently exhibits saddle behavior.

- **Points  $P_{2\mp}$ :** This point has similar coordinates to the previous point; however, the temperature parameter can take any value. This point also exhibits dynamics similar to the aforementioned point. After applying similar conditions, i.e.,  $0.9 < \Omega_\phi < 1$  and  $0 < \Omega_M < 0.1$ , the model parameters need to be fine-tuned in  $\beta$  and  $\delta$  as follows:

$$P_{2-}: \quad 0.816\sqrt{\delta^2 + 1.0} \leq \beta < 0.472\sqrt{3.0\delta^2 + 5.0} + 0.944, \quad (\delta > 24.50, \delta < -24.49),$$

$$P_{2+}: \quad 1.0 - 0.817\sqrt{\delta^2} < \beta < 1.0 - 0.577\sqrt{2.0\delta^2 + 3.0}, \quad (\delta > 23.24, \delta < -23.24).$$

This point also exhibits saddle-type behavior.

- **Point  $P_3$ :** At this point, the kinetic term of the field vanishes, and  $\xi$  can take any value. With a non-zero potential term the effective equation of state becomes  $-1$ , representing the late-time state of the universe. At this point, both the field and fluid fractional energy densities are finite. To constrain the model parameters, we argue that if the model drives late-time cosmic acceleration, the field fractional density must dominate over the fluid energy density, i.e.,  $0.5 \leq \Omega_\phi \leq 1$  and  $0 < \Omega_M < 0.4$ . This constrains  $(\lambda, \delta)$  for various choices of  $\beta$  as shown in Fig. [1a]. Note that  $(\beta = 0, 1)$  do not follow these constraints and are thus excluded from our analysis.

TABLE II: The conditions for the existence of the fixed points corresponding to Tab. [I] and their nature. The dashed lines refer to the discussion in the text.

$s_* = 0$					
Points	$\Omega_\phi$	$\Omega_M$	$\omega_{\text{eff}}$	$(\chi, \xi \geq 0)$	Stability
$P_{1-}$	$\frac{\left(\sqrt{6(\beta-1)^2-4\delta^2+\sqrt{6}(-\beta)+\sqrt{6}}\right)^2}{4\delta^2}$	$\frac{(\beta-2)\left(\sqrt{9(\beta-1)^2-6\delta^2-3\beta+3}\right)}{\delta^2} + 2$	-1	$\gamma < 0, \beta \leq 1 - \sqrt{\frac{2}{3}}\sqrt{\delta^2}$ $\gamma > 0, \beta > \sqrt{\frac{2}{3}}\sqrt{\delta^2} + 1$	-
$P_{1+}$	$\frac{\left(\sqrt{3(\beta-1)^2-2\delta^2+\sqrt{3}\beta-\sqrt{3}}\right)^2}{2\delta^2}$	$2\frac{\left(\sqrt{9(\beta-1)^2-6\delta^2+\delta^2-3}\right)-\beta\left(\sqrt{9(\beta-1)^2-6\delta^2+3\beta-9}\right)}{\delta^2}$	-1	$\gamma < 0, \beta \leq 1 - \sqrt{\frac{2}{3}}\sqrt{\delta^2}$ $\gamma > 0, \beta \geq \sqrt{\frac{2}{3}}\sqrt{\delta^2} + 1$	-
$P_{2-}$	$\frac{\left(\sqrt{9(\beta-1)^2-6\delta^2-3\beta+3}\right)^2}{6\delta^2}$	$\frac{(\beta-2)\left(\sqrt{9(\beta-1)^2-6\delta^2-3\beta+3}\right)}{\delta^2} + 2$	-1	$\gamma < 0, \beta \leq 1 - \sqrt{\frac{2}{3}}\sqrt{\delta^2}$ , $\gamma > 0, \beta \geq \sqrt{\frac{2}{3}}\sqrt{\delta^2} + 1$	-
$P_{2+}$	$\frac{\left(\sqrt{9(\beta-1)^2-6\delta^2+3\beta-3}\right)^2}{6\delta^2}$	$2\frac{\left(\sqrt{9(\beta-1)^2-6\delta^2+\delta^2-3}\right)-\beta\left(\sqrt{9(\beta-1)^2-6\delta^2+3\beta-9}\right)}{\delta^2}$	-1	$\gamma < 0, \beta \leq 1 - \sqrt{\frac{2}{3}}\sqrt{\delta^2}$ $\gamma > 0, \beta \geq \sqrt{\frac{2}{3}}\sqrt{\delta^2} + 1$	-
$P_3$	$\frac{\delta}{(\beta-1)\lambda+\delta}$	$\frac{\beta\lambda}{(\beta-1)\lambda+\delta}$	-1	$\lambda > 0, \gamma > 0, \beta > \frac{\lambda-\delta}{\lambda}$ $\lambda > 0, \gamma < 0, \beta < \frac{\lambda-\delta}{\lambda}$	-
$P_{4\mp}$	1	0	1	Satisfied	Unstable
$P_5$	1	$\frac{3\beta+\delta\lambda-3}{\delta^2}$	$\frac{\lambda-\beta\lambda}{\delta} - 1$	Fig. [2a]	Saddle
$P_6$	$\frac{3}{\lambda^2}$	$1 - \frac{3}{\lambda^2}$	0	Satisfied	Saddle
$P_7$	1	0	$\frac{1}{3}(\lambda^2 - 3)$	Satisfied	Saddle
$P_8$	$x_*^2 + y_*^2$	0	$\beta - \beta(x_*^2 + y_*^2) + 2x_*^2 - 1$	$-1 + x_*^2 + y_*^2 < 0, \alpha_1 > 0,$ $-1 + x_*^2 + y_*^2 > 0, \alpha_1 < 0.$	-
$P_9$	$x_*^2 + y_*^2$	$1 - (x_*^2 + y_*^2)$	$x_*^2 - y_*^2$	Satisfied	-

In addition to the density constraint, it is essential that the point yields real values and corresponding thermodynamic variable  $\chi$  remains positive, as per Eq. (5.9). The conditions for this are given in Tab. [II] and are also shown in Fig. [1a].

To further constrain the other model parameters, we evaluate the stability of the critical point by assuming various  $\beta$  values and fixing  $\alpha_1 = 1, \xi = 1$  as shown in Figs. [1b, 1c, 1d] for  $(\beta = 2, 3, -1)$  respectively. We find that in each case, one of the real parts of the eigenvalues becomes zero, while the rest take negative and positive values. Consequently, stability cannot be established using the linearization technique alone. Hence, to determine the stability of this point, we will employ a numerical technique. We will evolve the system near this fixed point by varying the initial conditions and model parameters and observing the convergence of the family of curves. If the curves do not converge to this point, it will be classified as a saddle or unstable point.

- **Points  $P_{4\mp}$ :** At these points, only the kinetic part of the field is non-zero, and the corresponding field density dominates over the fluid density. Since the effective equation of state is 1, these points exhibit stiff matter characteristics during the very early epoch of the universe. As explained earlier, these points represent the minimal coupling scenario for the quintessence field with an exponential type of potential, as  $z$  vanishes. These points always show unstable behavior.
- **Point  $P_5$ :** At this point, all the dynamical variables are non-zero except  $\xi$ . Correspondingly, the field density dominates, while the fluid density takes on a finite value depending on the model parameters. The effective equation of state also depends on the model parameters. We can constrain the model parameters  $(\delta, \lambda)$  by imposing the conditions  $0 < \Omega_M < 0.4$ ,  $-1.5 < \omega_{\text{eff}} < -1/3$ , and  $\chi > 0$ . The region of existence is shown in Fig. [2a] for values of

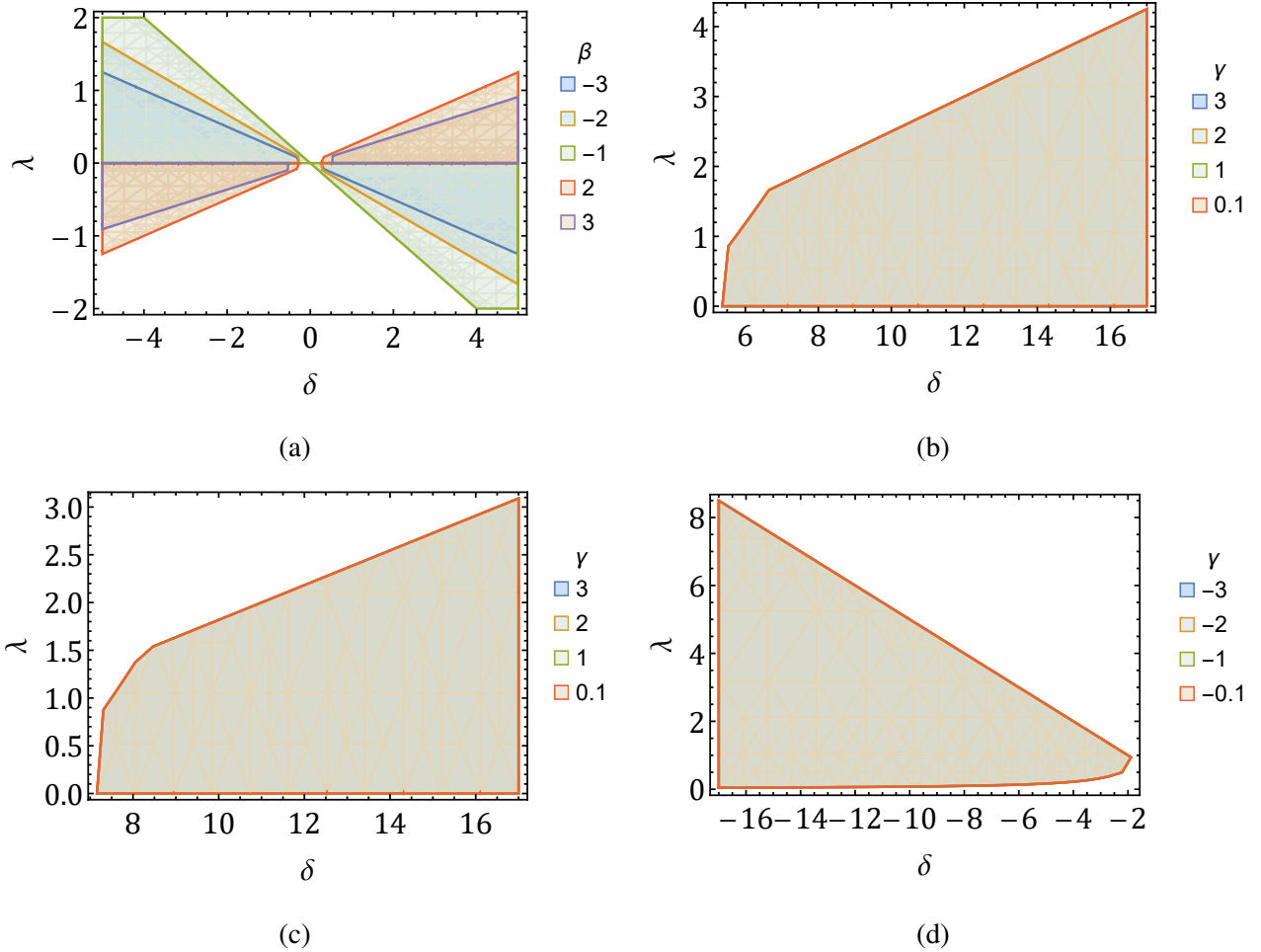
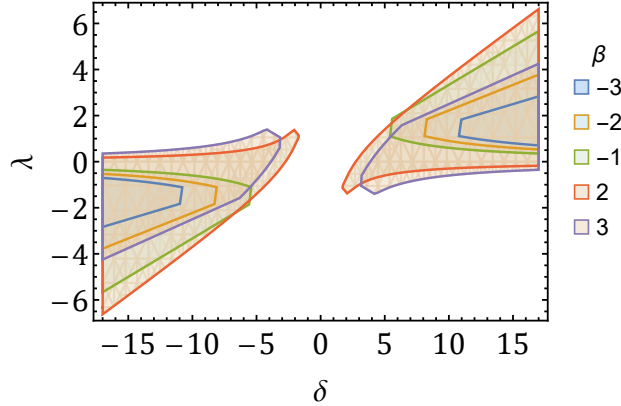


FIG. 1: (a) The region of existence corresponding to the fixed point  $P_3$ , assuming the constraints  $0.5 \leq \Omega_\phi \leq 1$  and  $0 < \Omega_M < 0.4$  for various choices of  $\beta$ , ensuring  $\chi > 0$  and a real value for  $y$  (as it contains a square root term). Here, for  $\beta > 0$ , the corresponding  $\gamma > 0$ , and for  $\beta < 0$ ,  $\gamma$  takes negative values. (b) The stability of the critical points evaluated for  $\beta = 2, \alpha_1 = 1, \xi = 1$ , considering all the necessary constraints, where one of the eigenvalues becomes zero. (c) The stability for  $\beta = 3, \alpha_1 = 1, \xi = 1$ , with all the constraints, where one of the eigenvalues becomes zero. (d) The stability for  $\beta = -1, \alpha_1 = 1, \xi = 1$ , where one of the eigenvalues becomes zero. Note that due to the overlapping regions, the colors corresponding to different  $\gamma$  values cannot be distinguished.

$\beta$  ranging from negative to positive. Note that  $\beta = 0, 1$ , do not satisfy the above constraints. For  $\beta > 0$ , the point can exhibit both phantom and accelerating solutions, whereas for  $\beta < 0$ , it exhibits only an accelerating solution. In both cases, the model parameter  $\gamma$  must be greater than zero. Upon evaluating the stability for any  $\beta$  with the aforementioned constraints, this point consistently exhibits a saddle solution within the confined region. Hence, this point cannot be considered a viable fixed point for representing late-time cosmology.

- **Point  $P_6$ :** This point represents the minimally coupled quintessence case where only the field dynamical variables are non-vanishing. At this point, both the field and fluid fractional densities depend on  $\lambda$ . The point follows the constraint relation Eq. (5.4) for  $\lambda^2 > 3$ . The



(a)

FIG. 2: (a) The region of existence for the point  $P_5$  shown for  $-1.5 < \omega_{\text{eff}} < -1/3$  and  $0 < \Omega_M < 0.4$ , along with  $\chi > 0$  and  $\gamma > 0$  for negative and positive values of  $\beta$ . Here, negative  $\beta$  shows only accelerating  $-1.0 < \omega_{\text{eff}} < -1/3$  solution while  $\beta > 0$  exhibits both phantom  $-1.5 < \omega_{\text{eff}} < -1$  and accelerating solution for  $\gamma > 0$ .

effective equation of state is always zero, signifying pressureless fluid type characteristics. The point consistently exhibits saddle-type behavior for any model parameters.

- **Point  $P_7$ :** Similar to the previous point, the field variables are only dependent on the potential parameter  $\lambda$ . At this point, the field density dominates over the fluid density, and the corresponding effective equation of state (EoS) is  $\lambda$  dependent. For  $0 < \lambda^2 < 2$ , the model can exhibit an accelerating solution. The point consistently exhibits saddle-type behavior for any choice of model parameters.
- **Point  $P_8$ :** At this point, the coordinates  $(x, y, \xi)$  can take any values, constrained by Eq. (5.4). Consequently, the field energy density can vary between 0 and 1, while the fluid energy density vanishes and remains subdominant. Depending on the dynamical variables and model parameter  $\beta$ , this point can exhibit an accelerating solution for  $\beta > 0$ . For  $\beta < 0$ , the point shows both accelerating and phantom characteristics. This constraint on  $(x, y)$  is illustrated in Fig. [3a] for different values of  $\beta$ . The corresponding stability is plotted in Fig. [3b] for  $\beta < 0, \gamma > 0$ , as a demonstration corresponding to  $(x_* = 0.2, y_* = 0.8)$ , ensuring the model satisfies the aforementioned constraint. We found that some of the eigenvalues are zero, positive, and negative. A similar behavior is observed for  $\beta > 0$ . Therefore, we need to rely on numerical evolution to determine the stability conclusively.
- **Point  $P_9$ :** At this point, the dynamical variables corresponding to the field and  $\xi$  can take any value satisfying the constraints in Eqs. (5.4) and (5.9). The field density can either dominate or sub-dominate depending on the initial conditions and model parameters. The stability of this point cannot be inferred from linear stability analysis alone, necessitating numerical evolution of the system to determine stability conclusively. However, since both the interaction parameter  $z$  and the number density parameter  $\chi$  vanish, this point represents the minimally coupled scenario for the field-fluid model.

After carefully investigating the nature of the critical points, we found that the critical points where  $s = 0$  represent different epochs of the universe. Some of these critical points, specifically



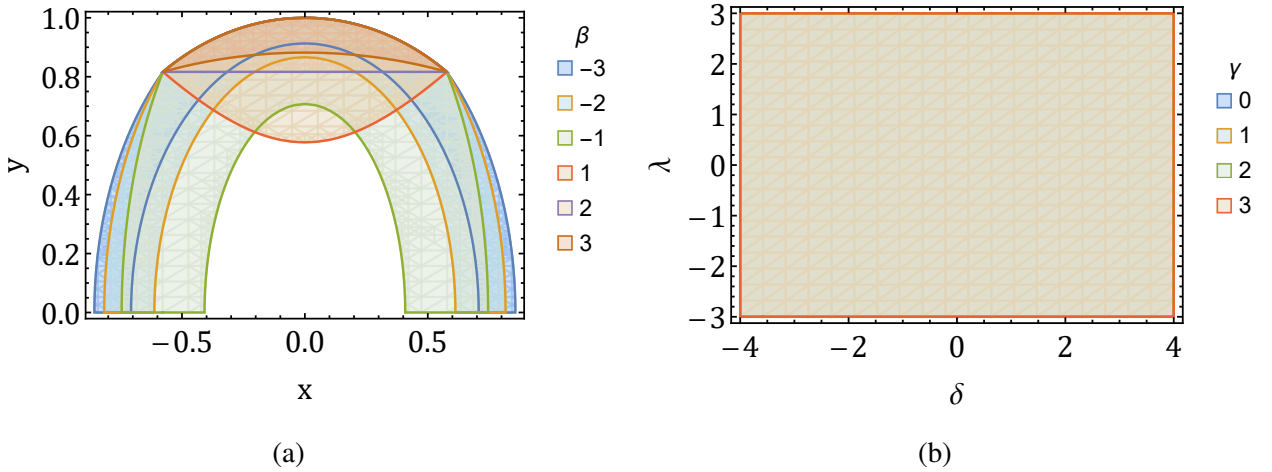


FIG. 3: (a) The region of existence for the point  $P_8$  with the field energy density  $0 < \Omega_\phi < 1$  and  $-1.5 < \omega_{\text{eff}} < -1/3$  for different choices of  $\beta$ . (b) The corresponding stability, where one of the eigenvalues is always zero for  $x_* = 0.2$ ,  $y_* = 0.8$ ,  $\beta = -1$ , cannot be concluded.

$P_1$  and  $P_2$ , may exhibit early-time accelerating phenomena. However, the existence conditions of these points indicate the need for fine-tuning of the model parameters  $\beta$  and  $\delta$ . Upon evaluating their stability, these points consistently yield saddle behavior.

There are various other critical points where the potential of the field is non-zero and exhibits an accelerating solution. Points  $P_3$  and  $P_8$ , which exert an accelerating solution, may become attractor points. Since the linearization technique cannot be adopted to determine their stability, numerical evolution of the system is necessary to ascertain the behavior of these points. In the subsequent section, we will present the numerical analysis corresponding to  $\beta \geq 0$ .

### A. Model corresponding to $\beta > 0$

In this section, we will study the system's stability and evolution corresponding to the interacting model  $f \propto \rho^2$ , where  $\beta = 2$ . From the above examination of the critical points, we determined that, the critical points corresponding to the interacting scenario, where  $z$ ,  $\chi$  is finite, the stability can not be inferred through the linearization technique. Hence, we will study the system numerically and determine the stable fixed point. To evolve the system numerically, we will choose only those model parameters where the accelerating critical points  $P_{3,5}$  exists. From the existence relations of  $P_{3,5}$  points in Figs. [1a, 2a], the critical points become valid for  $\beta \geq 2$ , hence we are carrying the analysis for  $\beta = 2$ . For the numerical evolution, we select  $\alpha_1 = 1$ , as the magnitude of  $\alpha_1$  does not alter the dynamics. Upon choosing the model parameters corresponding to the existence of point  $P_3$  from Fig. [1a] as follows:

$$\beta = 2, \alpha_1 = 1, \gamma = 2, \delta = 0.95, \lambda = 0.3, \quad (5.18)$$

the coordinates of the fixed point  $P_3$  become:  $(x = 0, y = 0.87, z = -0.24, \chi = 0.16, \xi = \xi_*, s = 0)$  and the corresponding field-fluid densities are:  $\Omega_\phi = 0.76$ ,  $\Omega_M = 0.48$ . In this parameter range, the point  $P_3$  does not stabilize, whereas the stability of the point  $P_8$  cannot be inferred as one of the eigenvalues becomes zero. Hence, to determine the stability of the critical point, we evolve the

system in the following range of model parameters and initial conditions. The range is given as:

$$\beta = 2, 0.08 < x_0 < 0.3, 0.8 < y_0 < 0.93, -0.2 < z_0 < -0.003, 0.01 < \chi_0 < 0.35, \quad (5.19)$$

$$\xi_0 = 1, 1.5 < \gamma < 2, 0.1 < \lambda < 0.9, 0.4 < \delta < 0.9, s_0 = 10^{-5}, 66 < H_0 < 76.$$

Here, the range of model parameters are considered near to Eq. (5.18). We will then generate the random numbers in this range and evolve the system. Here, we have fixed ( $\beta$ ) and ( $s_0$ ). The evolution of dynamical variables are plotted against the redefined time variable ( $\tilde{N}$ ) as shown in Fig. [4]. Here, we have taken the range of initial conditions at the present epoch ( $\tilde{N} = 0$ ), denoted by the subscript 0. From evolution of dynamical variables it can be seen that in the late-time epoch, i.e. ( $\tilde{N} > 0$ ), the curves corresponding to the dynamical variables stabilizes to  $P_8$ . From the evolution, one can see that in the past epoch, i.e., ( $\tilde{N} < 0$ ), the variable ( $z, \chi, s$ ) are non-zero, however, in the future epoch, these variables are saturating to 0. Throughout the evolution, we observe that the thermodynamic variables ( $\chi, \xi, s$ ) are either zero or positive, adhering to the constraint given by Eq. (5.9) on the system. Correspondingly, we have also plotted the cosmological parameters, for instance, the field density  $\Omega_\phi$ , effective equation of state  $\omega_{\text{eff}}$ , the Hubble parameter  $H(\tilde{z})$  and distance modulus  $\mu(\tilde{z})$  in Fig. [5]. Here ( $\tilde{z}$ ) represents the redshift,  $a = 1/(1 + \tilde{z})$ . To obtain the Hubble evolution, we use the following equation:

$$\frac{dH}{d\tilde{z}} = \frac{3}{2} \frac{1}{(1 + \tilde{z})} H(\tilde{z})(1 + \omega_{\text{eff}}). \quad (5.20)$$

Here, one requires to solve the autonomous equations with respect to the usual time variable i.e.,  $N = \ln a$  not  $\tilde{N}$ . As we are evaluating the dynamics for actual time variable  $N$ , however, as long as the system is far from  $\chi \rightarrow 0$ , the system produces similar dynamics as  $\tilde{N}$ . The distance modulus is defined as:

$$\mu = 5 \log_{10}(d_L) + 25, \quad (5.21)$$

where the luminosity distance is given by,

$$d_L = 2.99 \times 10^5 (1 + \tilde{z}) \int_0^{\tilde{z}} \frac{1}{H(\tilde{z})} d\tilde{z}. \quad (5.22)$$

For both the Hubble and distance modulus evolution, we have represented the plots against the (43) observational Hubble data and (1701) pantheon+ data ([url](#)) datasets [95, 96]. The deviation of the current model has been shown by comparing the curves with the best fit value obtained for  $\Lambda$ CDM model. From the evolution of cosmological parameters shown in Fig. [5], we observe that the effective equation of state in the current epoch is in the accelerating regime, with the scalar field density dominating. The Hubble evolution reveals that the curves grow faster compared to  $\Lambda$ CDM in the higher redshift regime, due to the increase of  $\chi$  in the past epoch. The incremental behavior of  $\chi$  and  $z$  in the past epoch causes the corresponding field energy density to increase, preventing the field component from vanishing entirely. Although the Hubble evolution plot shows apparent deviations, the distance modulus ( $\mu$ ) plot does not exhibit significant deviations.

We plot the cosmological parameter and the Hubble parameter against the redshift  $\tilde{z}$  in Figs. [6a] and [6b], corresponding to the best-fit values obtained in Tab. [III] using the data analysis technique. It can be seen that the dark matter density in the past ( $0.5 < \tilde{z} < 10$ ) is finite and dominates for some period. In the extreme past, the field energy density dominates again, whereas the dark matter density  $\Omega_M$  decreases and the corresponding effective and field EoS saturate to 1, showing stiff matter behavior. In the current epoch, the field energy density dominates over the

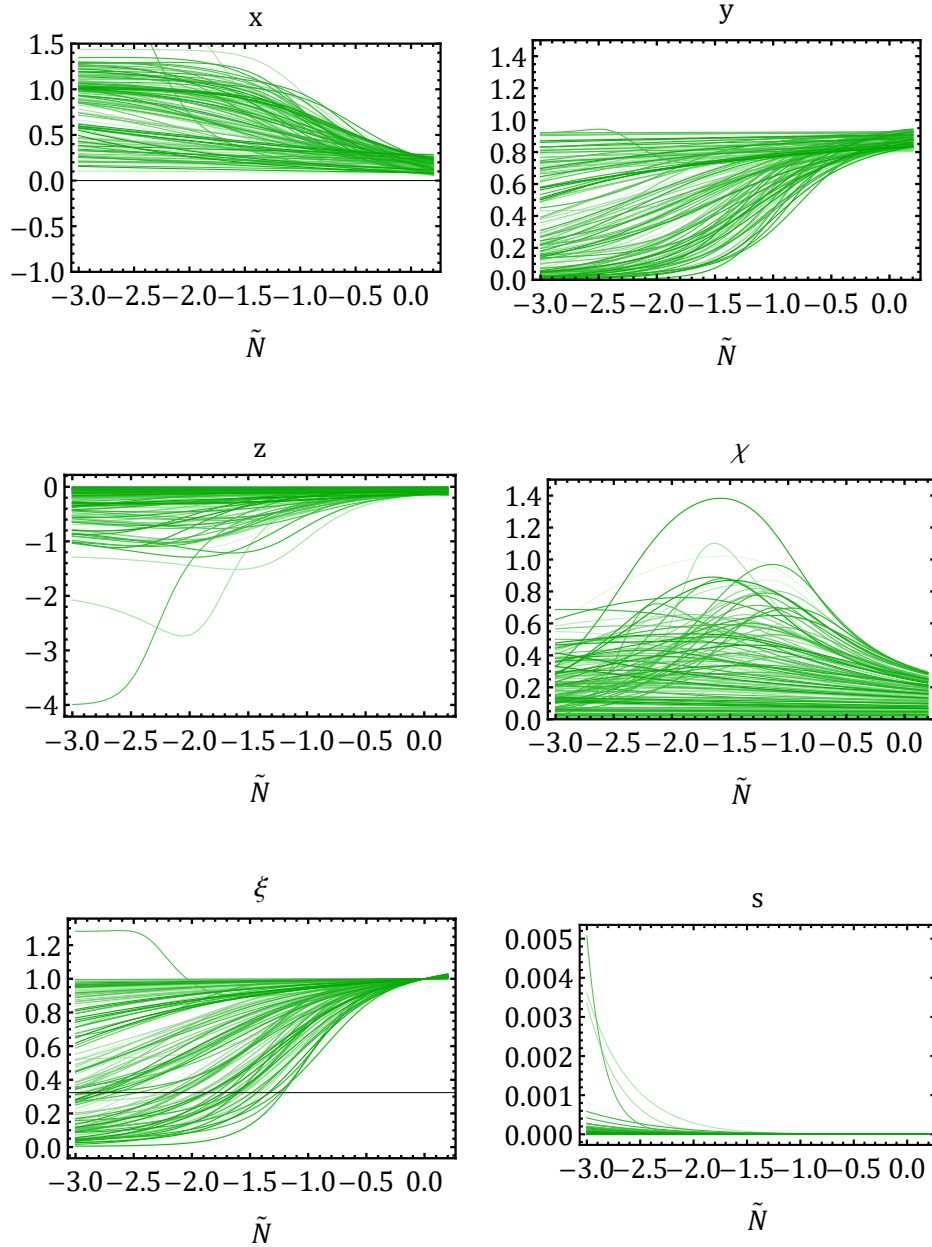


FIG. 4: The evolution of dynamical variables corresponding to the various choices of initial conditions and model parameters corresponding to  $\beta = 2$ .

fluid energy density, and the corresponding effective EoS is approximately  $-0.7$ . From the Hubble evolution plot, it can be seen that the current model produces behavior similar to the  $\Lambda$ CDM model.

### B. Model corresponding to $\beta < 0$

In this section, we will present a numerical analysis corresponding to the interacting model where  $\beta = -1$ . For this choice, we will use the model parameters near to the existence of  $P_3$  and

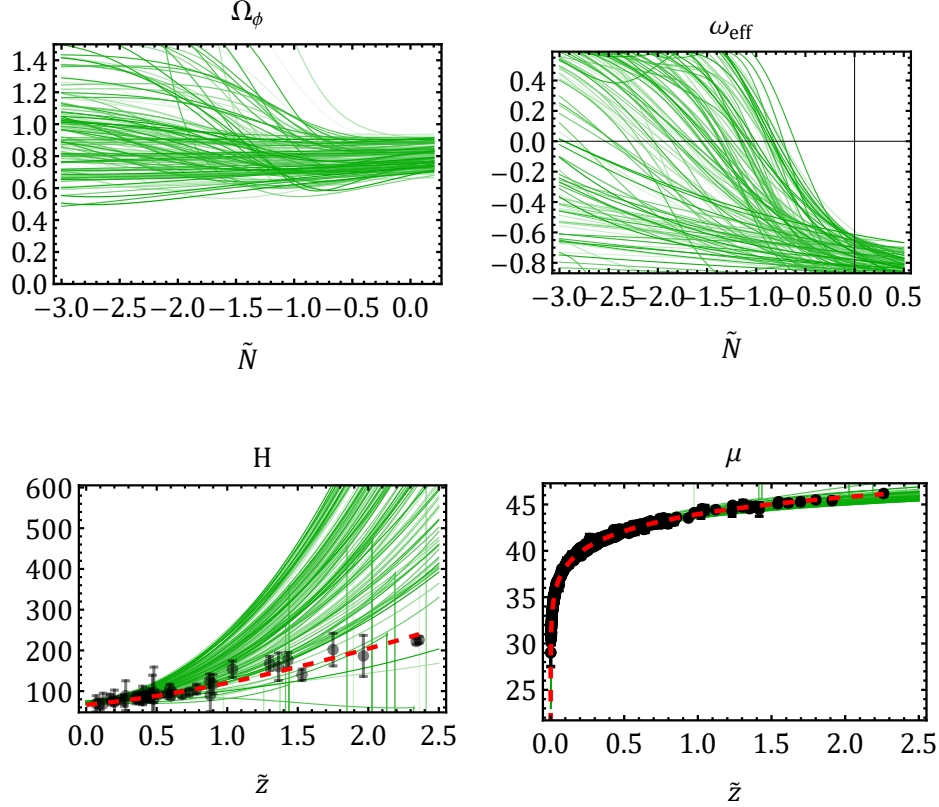


FIG. 5: The evolution of cosmological parameters for different initial conditions and model parameters corresponding to  $\beta = 2$ . Here in the  $H(\tilde{z})$  evolution, the red dashed line is corresponding to the  $\Lambda$ CDM model the best fit  $H_0 = 66.49$  km/s/Mpc,  $\Omega_\Lambda = 0.675$  obtained in [97] for Planck+Pantheon+ (without SH0ES). For the distance modulus ( $\mu$ ) plot, we have used the SH0ES best fit value for flat  $\Lambda$ CDM:  $H_0 = 73.6$  km/s/Mpc,  $\Omega_\Lambda = 0.666$

evolve the system. The range of model parameters and initial conditions are as follows:

$$\beta = -1, 0.08 < x_0 < 0.3, 0.7 < y_0 < 0.93, 0.02 < z_0 < 0.3, 0.05 < \chi_0 < 0.7, \xi_0 = 2, \quad (5.23)$$

$$0.5 < \gamma < 3, 0.5 < \lambda < 0.9, 0.4 < \delta < 3, 0.01 < s_0 < 0.5, 66 < H_0 < 76.$$

The evolution of the dynamical variables is plotted in Fig. [7]. From the plot, it can be seen that in the past epoch, the variable  $z$  vanishes, indicating  $H \gg f$ , while  $s$  vanishes for some initial conditions and model parameters. However, in the current epoch,  $z$  becomes finite but again vanishes in the far future epoch, whereas the entropy saturates to a finite value. The variable  $\chi$  takes a finite value in the past epoch but vanishes in the future. This indicates that in the far future, the particle production phenomenon freezes as the source term of Eq. (3.7) vanishes, and the entropy per particle density becomes constant. Throughout the evolution,  $\xi$  remains positive and eventually saturates in the future. However, some abrupt changes are observed for certain combinations of model parameters, which can be discarded. The value of  $x$  is positive in the past but saturates to near zero, both negatively and positively, while  $y$  saturates near 1. Hence, the system is saturating to some fixed point where  $(z, \chi = 0)$  and  $(\xi, s \neq 0)$  can take any positive value. This behavior closely resembles point  $P_9$ ; however, at this point, both  $s$  and  $z$  are zero. Therefore, there exists another critical point, labeled as  $P_{10}$ , similar to  $P_9$ , where  $z$  vanishes while  $s$  can take any positive

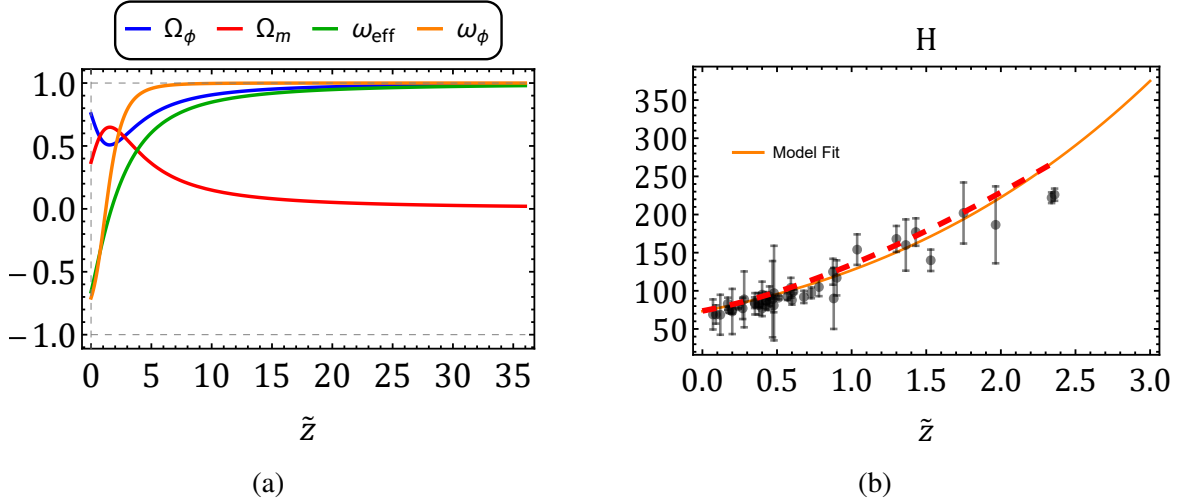


FIG. 6: (a) The evolution of the system corresponding to  $\beta = 2$ , for the best fit value obtained in Tab. [III] where  $\alpha_1 = 1, \gamma = 1, \delta = 1.87, \lambda = -0.558$ , with  $x(0) = 0.332, y(0) = 0.803, z(0) = -0.125, \chi(0) = 0.0998, \xi(0) = 1, s(0) = 10^{-2}$ . (b) The corresponding Hubble evolution is compared against  $\Lambda$ CDM (shown in red dotted line) for the best fit values of  $H_0 = 73.60$  km/s/Mpc,  $\Omega_\Lambda = 0.666$  obtained in [97] for Pantheon+ and SHOES data.

finite value. Note that this point is not indexed in Tab. [I]. The coordinates corresponding to this point are  $P_{10} = (\text{Any}, \text{Any}, 0, 0, \text{Any}, \text{Any})$ . The dynamical behavior shows that within a certain range of model parameters, this point becomes stable.

The corresponding cosmological parameter evolution is shown in Fig. [8], where the effective equation of state at the current epoch is in the accelerating regime and transitions to the phantom regime  $\omega_{\text{eff}} < -1$  in the future epoch for a brief period. During this period, the interaction variable  $z$  becomes non-zero, and the field density remains constrained to  $0 < \Omega_\phi < 1$ . However, as the system further evolves into the far future epoch, it eventually transitions to an accelerating phase with  $-1 < \omega_{\text{eff}} < -0.5$ , and  $z$  vanishes. In the past, the field energy density becomes greater than 1 for some initial conditions and model parameters, signifying a non-physical scenario since  $z$  remains close to zero in the past epoch, making  $\Omega_m < 0$ . Hence, those benchmark points cannot be considered viable.

Similar to the previous case, we have plotted the cosmological parameters using the best-fit values obtained in Tab. [III] in Figs. [9a, 9b]. The matter density dominates in the past for certain redshifts; however, at high redshifts, the field density dominates, and the corresponding effective equation of state (EoS) becomes 1, signifying stiff matter behavior. Unlike the previous case, here the matter energy density remains finite and dominant for a very long interval of redshift, and the corresponding effective EoS also vanishes, resulting in a definite matter-dominated epoch. On the other hand, due to this extended domination period of matter, we see a clear deviation in the Hubble plot from the  $\Lambda$ CDM model. At the current epoch, the field energy density dominates with  $\Omega_\phi = 87\%$  and matter energy density  $\Omega_{M0} = 45\%$ . Although the model shows better fitting with the data, we see an abrupt change in behavior around  $\tilde{z} < 0$ . This could be due to the fact that we use the autonomous system of equations corresponding to the usual time variable  $N$  rather than  $\tilde{N}$ . The evolution of the EoS signifies that the system transitions from non-accelerating to accelerating regime, however, as the system further progresses into the future epoch  $\tilde{z} < 0$ , the EoS increases,

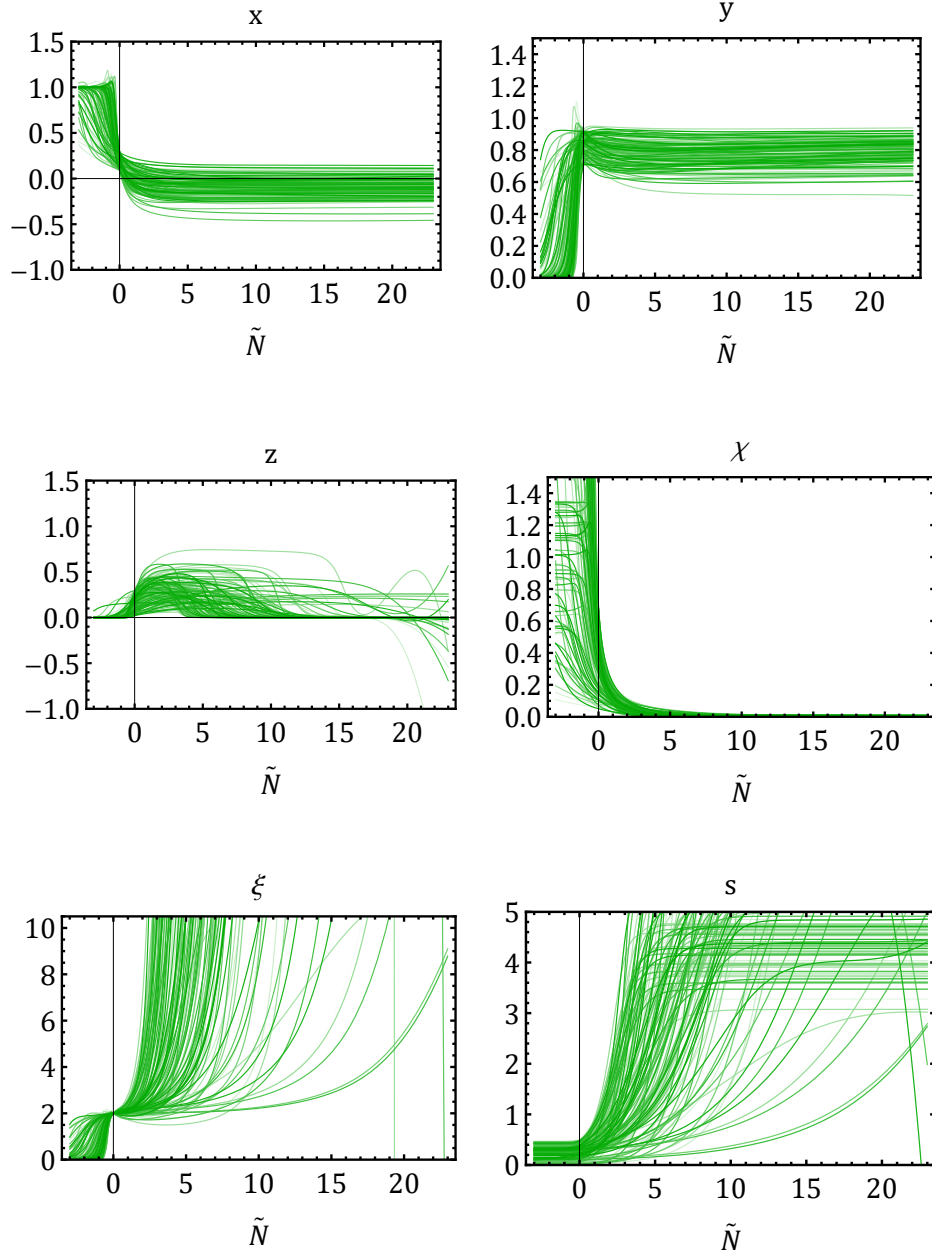


FIG. 7: The evolution of dynamical variables for various initial conditions and model parameters corresponding to  $\beta = -1$ .

making the system non-accelerating.

We discuss the data analysis technique used to obtain the best-fit values of the model parameters in the next section.

## VI. DATA ANALYSIS

In this section, we will obtain constraints on the parameter space of the predefined models. We utilize the recently released SNe Ia distance moduli ( $\mu$ ) measurements from the Pantheon+ and

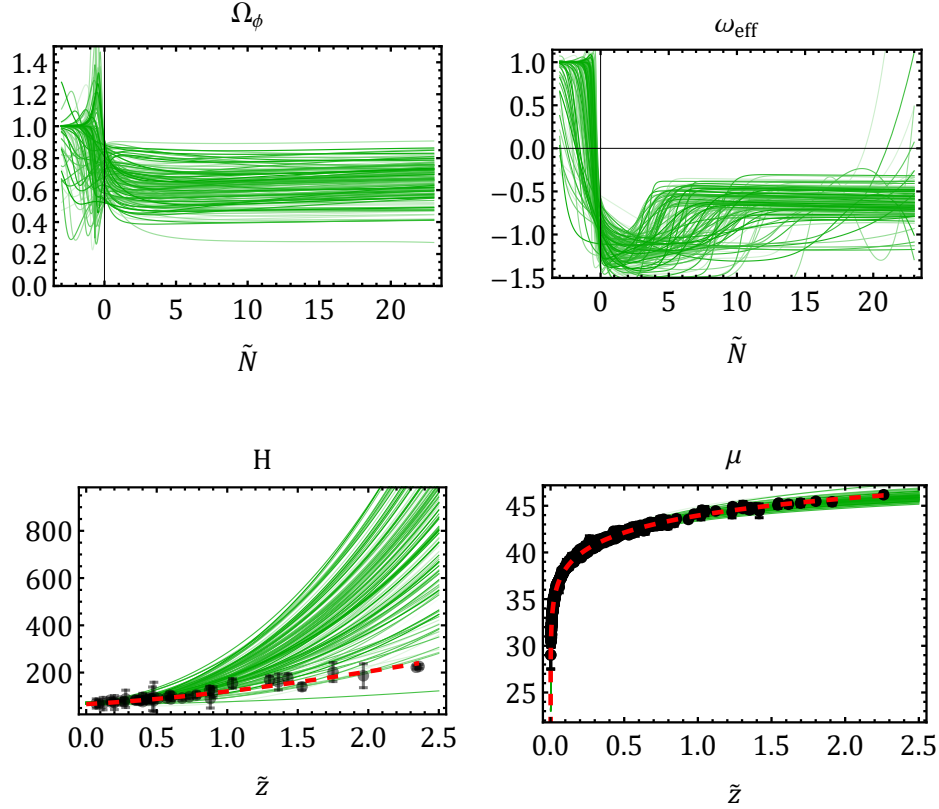


FIG. 8: The evolution of cosmological parameters for different initial conditions and model parameters corresponding to  $\beta = -1$ . In the  $H(\tilde{z})$  evolution, the red dashed line corresponds to the  $\Lambda$ CDM model with the best fit  $H_0 = 66.49$  km/s/Mpc and  $\Omega_\Lambda = 0.675$  obtained in [97] for Planck+Pantheon+ (without SHOES). For the distance modulus  $\mu$  plot, we have used the SHOES best fit value for flat  $\Lambda$ CDM:  $H_0 = 73.6$  km/s/Mpc and  $\Omega_\Lambda = 0.666$ .

SHOES sample, which consists of 1701 light curves of 1550 supernovae observed in the redshift range  $z \in [0, 2.3]$  [97]. The distance modulus corresponding to the model is computed using:

$$\mu_{\text{Model}} = 5 \log_{10}(d_L) + 25, \quad (6.1)$$

where the luminosity distance  $d_L$  is given by,

$$d_L = 2.99 \times 10^5 (1 + \tilde{z}) \int_0^{\tilde{z}} \frac{1}{H(\tilde{z})} d\tilde{z}. \quad (6.2)$$

To constraint the parameter space, we follow the standard  $\chi^2$  analysis technique.<sup>2</sup> By minimizing the  $\chi^2$  likelihood, defined as:

$$\chi_{\text{SN}}^2 = -2 \ln(\mathcal{L}) = \Delta \mathbf{D}^T \mathbf{C}_{\text{stat+sys}}^{-1} \Delta \mathbf{D} \quad (6.3)$$

<sup>2</sup> Note that here,  $\chi$  is not a dynamical variable defined in Eq. (5.8).

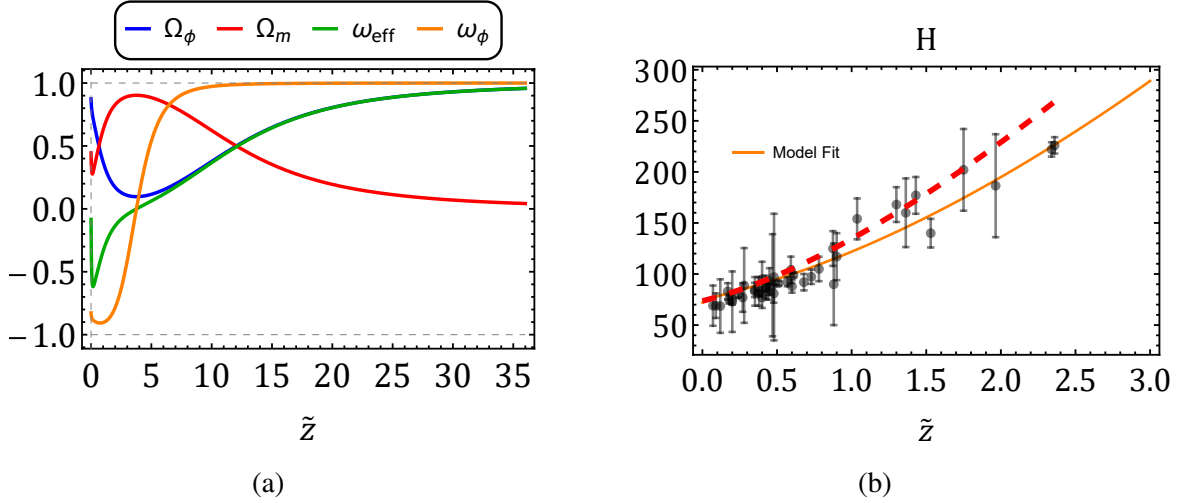


FIG. 9: The evolution of the composite system corresponding to  $\beta = -1$ , fitted for the best value obtained in Tab. [III], where  $\alpha_1 = 1, \gamma = 1, \delta = 2.6, \lambda = -0.78$ , with  $x(0) = 0.275, y(0) = 0.894, z(0) = -0.32, \chi(0) = 0.0245, \xi(0) = 1, s(0) = 0.1$ . (b). The Hubble evolution has been obtained against  $\Lambda$ CDM for the best fit  $H_0 = 73.60$  km/s/Mpc,  $\Omega_\Lambda = 0.666$  obtained in [97] for Pantheon+ and SHOES.

where  $\Delta \mathbf{D}$  is a column matrix of residual of distance modulus:

$$\Delta \mathbf{D} = \mu_{\text{data}} - \mu_{\text{Model}}. \quad (6.4)$$

Here,  $C_{\text{stat+sys}} = C_{\text{stat}} + C_{\text{sys}}$  denotes the combined statistical and systematic  $1701 \times 1701$  covariance matrix.

We utilize another dataset, namely the observational Hubble data (OHD), which comprises 43 data points in the redshift range  $\tilde{z} \in [0.07, 2.36]$  [95, 98]. In this dataset, 31 data points are obtained using a model-independent analysis called Cosmic Chronometers (CC), and the rest are obtained from the Baryon Acoustic Oscillation (BAO) measurements, assuming the standard cosmology. The corresponding  $\chi^2$  likelihood is defined as:

$$\chi_{\text{OHD}}^2 = \sum_{i=1}^{43} \frac{(H_i^{\text{obs}} - H_i^{\text{Model}})^2}{\sigma_i^2}. \quad (6.5)$$

Here,  $\sigma_i$  denotes the uncertainty in each Hubble observational data point. The best-fit parameters are obtained by minimizing the total  $\chi^2$ :

$$\chi_{\text{tot}}^2 = \chi_{\text{SN}}^2 + \chi_{\text{OHD}}^2. \quad (6.6)$$

To obtain the Hubble evolution, we use Eq. (5.20). We apply uniform priors for all parameters, summarized in Table [III]. Note that the dashed marks in the prior row indicate that the variable has not been constrained. The publicly available Python package ‘dynesty,’ a Dynamical Nested Sampling Package, is employed to estimate Bayesian posteriors and evidences [99–102]. Dynesty is a Python implementation of the nested sampling algorithm, which is a powerful tool for exploring complex posterior distributions. The resulting posterior samples are further analyzed using the publicly available GetDist Python package, where  $1\sigma$  and  $2\sigma$  contours are generated [103]. The



TABLE III: Summary of the 68% confidence limits for each cosmological parameter. The parameters with indicated ranges are those fitted to the data.

Model	$H_0$	$x_0$	$y_0$	$z_0$	$\chi_0$	$\xi_0$	$s_0$	$\lambda$	$\gamma$	$\delta$	$\Omega_{M0}$
For $\beta = 2$											
Priors:	[30, 100]	-	[0.40, 0.95]	[-0.2, 0.2]	[0.0, 0.5]	1	-	[-0.7, 1.3]	-	[0, 4]	[0, 0.7]
Model I:	$73.32 \pm 0.22$	0.332	$0.803 \pm 0.039$	$-0.125^{+0.021}_{-0.072}$	$0.0998^{+0.034}_{-0.025}$	1	0.001	$-0.558^{+0.012}_{-0.14}$	1	$1.87^{+0.81}_{-1.1}$	$0.37^{+0.15}_{-0.11}$
For $\beta = -1$											
Priors:	[30, 100]	-	[0.4, 0.95]	[-0.6, 1]	[0, 0.5]	-	-	[-1.5, 2.0]	-	[-5, 7]	[0, 0.6]
Model II:	$72.20 \pm 0.33$	0.275	$0.894 \pm 0.021$	$-0.32^{+0.062}_{-0.10}$	$0.0245^{+0.0054}_{-0.014}$	1	0.1	$-0.78^{+0.19}_{-0.23}$	1	$2.6^{+4.2}_{-1.8}$	$0.445^{+0.12}_{-0.073}$

best-fit values of the parameters shown in the figures correspond to the 68% confidence level.

The contour plot corresponding to  $\beta = 2$  is shown in Fig. [10] with  $\alpha_1 = 1$ . To constrain the parameter space, we have fixed  $\xi_0 = 1$ ,  $s_0 = 0.001$ , and  $\gamma = 1$ . Note that  $x_0$  is not fixed. We have evaluated it using the constraint Eq. (5.2) as,

$$x_0 = \sqrt{1 - \Omega_{M0} - y_0^2 - \alpha_1 z_0}. \quad (6.7)$$

The best-fit values of the model are summarized in Tab. [III]. Based on these best-fit values, the scalar field density is ( $\Omega_{\phi 0} = x_0^2 + y_0^2 = 0.75$ ), the matter density is  $\Omega_{M0} = 0.37$  and the Hubble parameter becomes  $H_0 = 73.32$  km/s/Mpc. Some parameters were fixed because they do not significantly affect the overall evolution of the system. We also determined widely used information criteria to compare the models for evidence, including the Akaike Information Criterion (AIC) and the Bayesian Information Criterion (BIC) [104]. The AIC and BIC are defined as:

$$\begin{aligned} \text{AIC} &= -2 \ln \mathcal{L}_{\max} + 2k, \\ \text{BIC} &= -2 \ln \mathcal{L}_{\max} + k \ln N, \end{aligned} \quad (6.8)$$

where  $k$  is the number of independent parameters in the model,  $N$  represents the total number of data points, and  $\mathcal{L}_{\max}$  represents the maximum likelihood. For the  $\Lambda$ CDM model with the combined data sets, the AIC is 1840.10, and the BIC is 1851.03. The current model yields AIC = 1828.59 and BIC = 1866.83. To compare the models with  $\Lambda$ CDM, one can define the difference  $\Delta\text{IC} = \text{IC}(\text{Model}) - \text{IC}(\Lambda\text{CDM})$ , where IC denotes AIC and BIC. The range of  $\Delta\text{IC}$  is usually interpreted as follows:  $\Delta\text{IC} < 2$  indicates substantial support,  $4 < \Delta\text{IC} < 7$  indicates much less support, and  $\Delta\text{IC} > 10$  indicates essentially no support [105–107]. For the current model,  $\Delta\text{AIC} = -11.51$  and  $\Delta\text{BIC} = 15.8$ . Based on the AIC criterion, the current model shows strong support; however, based on the BIC criterion, it is not supported.

The best fit values corresponding to the model with  $\beta = -1$  has been shown in Fig. [11]. For this model we have fixed the parameters ( $s_0, \xi_0, \gamma$ ) and their corresponding values are summarized in Tab. [III]. We have fixed  $\alpha_1 = 1$ , since it does not affect the dynamics. The priors of the parameters and corresponding best fit values are summarized in Tab. [III]. The field density is  $\Omega_{\phi 0} = 0.87$ , fluid density is  $\Omega_{M0} = 0.45$  and the Hubble parameter is  $H_0 = 72.20$  km/s/Mpc. The model yields AIC= 1815.09, and BIC= 1853.34. The difference in IC becomes:  $\Delta\text{AIC} = -25.01$ , and  $\Delta\text{BIC} = 2.31$ . Negative AIC implies strong support for the current model, however, BIC does not show very strong support.

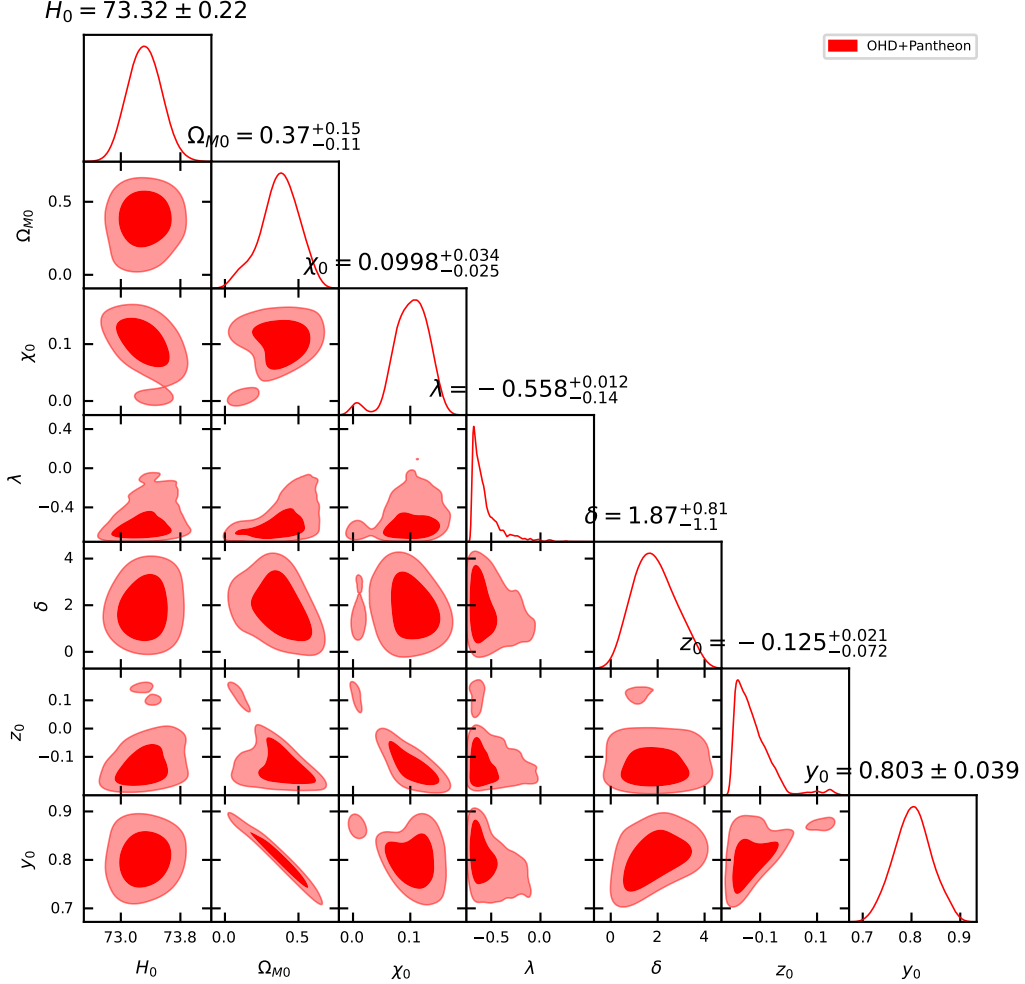


FIG. 10: The model  $\beta = 2$ , is fitted with OHD+Pantheon+ and SHOES data.

## VII. CONCLUSION

In this paper, a non-minimal coupling scenario between the quintessence field and a pressureless fluid is examined through the variational principle. The interaction function ( $f$ ) is introduced at a Lagrangian level, depending on both field and fluid degrees of freedom. A Lagrange parameter  $\varphi$  representing the thermodynamic variable corresponding to the gradient of chemical free energy ( $F$ ) is incorporated in  $f$ . This incorporation results in altered equations of motion for the number density and entropy per particle density. The interaction function ( $f$ ) serves as the source term for the production or annihilation of dark matter particles and entropy production, consequently altering the evolution of the fluid's temperature. Modeling the dark matter fluid as a pressureless ideal gas, the entropy becomes a logarithmic function of the temperature. Due to the non-minimal coupling function ( $f$ ), the covariant derivatives of the stress tensors of the individual components are no longer conserved, facilitating the flow of energy from the field to the fluid through the field derivative of the interaction function  $f_{,\phi}\dot{\phi}$ .

The equations of motion for the field and fluid are modified due to the non-minimal coupling scenario. The dynamics of the composite system require assuming a particular form of the interaction function, which depends on several field-fluid parameters, resulting in multiple free

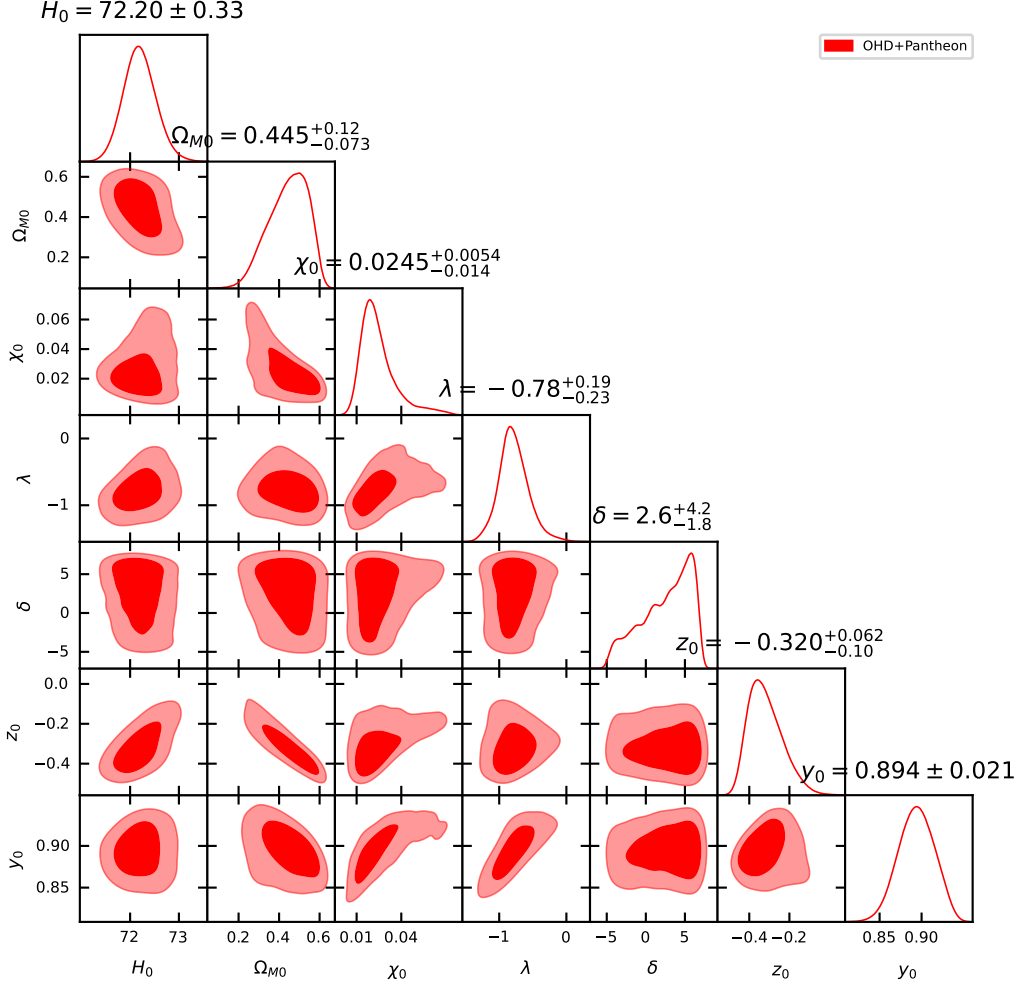


FIG. 11: The model  $\beta = -1$ , is fitted with OHD+Pantheon+ and SH0ES data.

parameters in the model. Constraining these model parameters is essential and has been explicitly discussed using the dynamical system stability technique. An exponential interaction model and an exponential potential for the quintessence field have been chosen for this study.

The system's stability has been assessed using the linearization technique corresponding to a 6-dimensional phase space, yielding 13 critical points categorized based on their physical characteristics to describe different phases (non-accelerating to accelerating) of the universe. Two models were particularly studied where the interaction function is  $f \propto \rho^2$  and  $f \propto \rho^{-1}$ . For these models, the parameters were constrained by evaluating the physical viability of the critical points. The physically viable critical points are those that generate accelerating or non-accelerating solutions, with field and fluid densities bound between 0 to 1. Additionally, these points must yield positive values for thermodynamic variables, such as the number density ( $\chi$ ), the temperature variable ( $\xi$ ), and entropy per particle density ( $s$ ). It was found that the stability of some critical points could not be evaluated using conventional linearization techniques, as one of the real parts of the eigenvalue becomes zero. Given the phase space dimension is more than 3, using mathematical tools like the center manifold theorem becomes extremely challenging. Therefore, the stability of those critical points was evaluated by numerically evolving the system near the critical points' existence by generating random numbers.

To determine the viability of the model parameters, the corresponding Hubble parameter ( $H$ ) and distance modulus ( $\mu$ ) were plotted alongside the  $\Lambda$ CDM model using 43 observational Hubble data points and 1701 Pantheon+ samples. The numerical simulation demonstrated that the current model can mimic  $\Lambda$ CDM behavior; however, the true best fit values can only be obtained using proper data analysis techniques.

A publicly available Python package, *dynesty*, implementing the Dynamical Nested Sampling method, was adopted to estimate the Bayesian posteriors and evidence. The model  $f \propto \rho^2$  yields  $H_0 = 73.32$  km/s/Mpc,  $\Omega_{M0} = 37\%$ , and  $\Omega_{\phi0} = 75\%$ , showing a similar  $H(\bar{z})$  evolution to  $\Lambda$ CDM. On the other hand, the model  $f \propto \rho^{-1}$  yields  $H_0 = 72.20$  km/s/Mpc,  $\Omega_{M0} = 45\%$ , and  $\Omega_{\phi0} = 87\%$ , but shows deviations at higher redshifts. The evidence of the current models was compared to  $\Lambda$ CDM using the Akaike Information Criterion (AIC) and Bayesian Information Criterion (BIC). For both current models, the  $\Delta$ AIC value shows strong support, while the  $\Delta$ BIC does not indicate very strong support.

## REFERENCES

---

- [1] S. Perlmutter *et al.* (Supernova Cosmology Project), Measurements of  $\Omega$  and  $\Lambda$  from 42 high redshift supernovae, *Astrophys. J.* **517**, 565 (1999), [arXiv:astro-ph/9812133](#).
- [2] A. G. Riess *et al.* (Supernova Search Team), Observational evidence from supernovae for an accelerating universe and a cosmological constant, *Astron. J.* **116**, 1009 (1998), [arXiv:astro-ph/9805201](#).
- [3] D. N. Spergel *et al.* (WMAP), First year Wilkinson Microwave Anisotropy Probe (WMAP) observations: Determination of cosmological parameters, *Astrophys. J. Suppl.* **148**, 175 (2003), [arXiv:astro-ph/0302209](#).
- [4] B. D. Sherwin *et al.*, Evidence for dark energy from the cosmic microwave background alone using the Atacama Cosmology Telescope lensing measurements, *Phys. Rev. Lett.* **107**, 021302 (2011), [arXiv:1105.0419 \[astro-ph.CO\]](#).
- [5] E. L. Wright, Constraints on Dark Energy from Supernovae, Gamma Ray Bursts, Acoustic Oscillations, Nucleosynthesis and Large Scale Structure and the Hubble constant, *Astrophys. J.* **664**, 633 (2007), [arXiv:astro-ph/0701584](#).
- [6] J. Kwan *et al.* (DES), Cosmology from large-scale galaxy clustering and galaxy–galaxy lensing with Dark Energy Survey Science Verification data, *Mon. Not. Roy. Astron. Soc.* **464**, 4045 (2017), [arXiv:1604.07871 \[astro-ph.CO\]](#).
- [7] T. M. C. Abbott *et al.* (DES), Dark Energy Survey Year 3 results: A 2.7% measurement of baryon acoustic oscillation distance scale at redshift 0.835, *Phys. Rev. D* **105**, 043512 (2022), [arXiv:2107.04646 \[astro-ph.CO\]](#).
- [8] D. Scolnic *et al.*, The Pantheon+ Analysis: The Full Data Set and Light-curve Release, *Astrophys. J.* **938**, 113 (2022), [arXiv:2112.03863 \[astro-ph.CO\]](#).
- [9] N. Aghanim *et al.* (Planck), Planck 2018 results. VI. Cosmological parameters, *Astron. Astrophys.* **641**, A6 (2020), [Erratum: *Astron. Astrophys.* 652, C4 (2021)], [arXiv:1807.06209 \[astro-ph.CO\]](#).
- [10] E. J. Copeland, M. Sami, and S. Tsujikawa, Dynamics of dark energy, *Int. J. Mod. Phys. D* **15**, 1753 (2006), [arXiv:hep-th/0603057](#).
- [11] S. Weinberg, The Cosmological Constant Problem, *Rev. Mod. Phys.* **61**, 1 (1989).

- [12] S. E. Rugh and H. Zinkernagel, The Quantum vacuum and the cosmological constant problem, *Stud. Hist. Phil. Sci. B* **33**, 663 (2002), [arXiv:hep-th/0012253](#).
- [13] T. Padmanabhan, Cosmological constant: The Weight of the vacuum, *Phys. Rept.* **380**, 235 (2003), [arXiv:hep-th/0212290](#).
- [14] S. M. Carroll, W. H. Press, and E. L. Turner, The Cosmological constant, *Ann. Rev. Astron. Astrophys.* **30**, 499 (1992).
- [15] N. Arkani-Hamed, L. J. Hall, C. F. Kolda, and H. Murayama, A New perspective on cosmic coincidence problems, *Phys. Rev. Lett.* **85**, 4434 (2000), [arXiv:astro-ph/0005111](#).
- [16] H. E. S. Velten, R. F. vom Marttens, and W. Zimdahl, Aspects of the cosmological “coincidence problem”, *Eur. Phys. J. C* **74**, 3160 (2014), [arXiv:1410.2509 \[astro-ph.CO\]](#).
- [17] E. Di Valentino, O. Mena, S. Pan, L. Visinelli, W. Yang, A. Melchiorri, D. F. Mota, A. G. Riess, and J. Silk, In the realm of the Hubble tension—a review of solutions, *Class. Quant. Grav.* **38**, 153001 (2021), [arXiv:2103.01183 \[astro-ph.CO\]](#).
- [18] C. Krishnan, E. O. Colgáin, Ruchika, A. A. Sen, M. M. Sheikh-Jabbari, and T. Yang, Is there an early Universe solution to Hubble tension?, *Phys. Rev. D* **102**, 103525 (2020), [arXiv:2002.06044 \[astro-ph.CO\]](#).
- [19] T. M. Davis, S. R. Hinton, C. Howlett, and J. Calcino, Can redshift errors bias measurements of the Hubble Constant?, *Mon. Not. Roy. Astron. Soc.* **490**, 2948 (2019), [arXiv:1907.12639 \[astro-ph.CO\]](#).
- [20] W. Yang, S. Pan, E. Di Valentino, R. C. Nunes, S. Vagnozzi, and D. F. Mota, Tale of stable interacting dark energy, observational signatures, and the  $H_0$  tension, *JCAP* **09**, 019, [arXiv:1805.08252 \[astro-ph.CO\]](#).
- [21] E. Di Valentino, A. Melchiorri, O. Mena, and S. Vagnozzi, Nonminimal dark sector physics and cosmological tensions, *Phys. Rev. D* **101**, 063502 (2020), [arXiv:1910.09853 \[astro-ph.CO\]](#).
- [22] R. C. Nunes, S. Vagnozzi, S. Kumar, E. Di Valentino, and O. Mena, New tests of dark sector interactions from the full-shape galaxy power spectrum, *Phys. Rev. D* **105**, 123506 (2022), [arXiv:2203.08093 \[astro-ph.CO\]](#).
- [23] S. Vagnozzi, New physics in light of the  $H_0$  tension: An alternative view, *Phys. Rev. D* **102**, 023518 (2020), [arXiv:1907.07569 \[astro-ph.CO\]](#).
- [24] T. P. Sotiriou and V. Faraoni,  $f(R)$  Theories Of Gravity, *Rev. Mod. Phys.* **82**, 451 (2010), [arXiv:0805.1726 \[gr-qc\]](#).
- [25] S. Nojiri and S. D. Odintsov, Introduction to modified gravity and gravitational alternative for dark energy, *eConf C0602061*, 06 (2006), [arXiv:hep-th/0601213](#).
- [26] J. Beltrán Jiménez, L. Heisenberg, and T. Koivisto, Coincident General Relativity, *Phys. Rev. D* **98**, 044048 (2018), [arXiv:1710.03116 \[gr-qc\]](#).
- [27] Y.-F. Cai, S. Capozziello, M. De Laurentis, and E. N. Saridakis,  $f(T)$  teleparallel gravity and cosmology, *Rept. Prog. Phys.* **79**, 106901 (2016), [arXiv:1511.07586 \[gr-qc\]](#).
- [28] P. J. E. Peebles and B. Ratra, The Cosmological Constant and Dark Energy, *Rev. Mod. Phys.* **75**, 559 (2003), [arXiv:astro-ph/0207347](#).
- [29] T. Nishioka and Y. Fujii, Inflation and the decaying cosmological constant, *Phys. Rev. D* **45**, 2140 (1992).
- [30] C. Armendariz-Picon, V. F. Mukhanov, and P. J. Steinhardt, A Dynamical solution to the problem of a small cosmological constant and late time cosmic acceleration, *Phys. Rev. Lett.* **85**, 4438 (2000), [arXiv:astro-ph/0004134](#).
- [31] C. Armendariz-Picon, V. F. Mukhanov, and P. J. Steinhardt, Essentials of  $k$  essence, *Phys. Rev. D* **63**, 103510 (2001), [arXiv:astro-ph/0006373](#).
- [32] T. Chiba, T. Okabe, and M. Yamaguchi, Kinetically driven quintessence, *Phys. Rev. D* **62**, 023511

- (2000), [arXiv:astro-ph/9912463](#).
- [33] A. Y. Kamenshchik, U. Moschella, and V. Pasquier, An Alternative to quintessence, *Phys. Lett. B* **511**, 265 (2001), [arXiv:gr-qc/0103004](#).
- [34] M. C. Bento, O. Bertolami, and A. A. Sen, Generalized Chaplygin gas, accelerated expansion and dark energy matter unification, *Phys. Rev. D* **66**, 043507 (2002), [arXiv:gr-qc/0202064](#).
- [35] J. R. Ellis, S. Kalara, K. A. Olive, and C. Wetterich, Density Dependent Couplings and Astrophysical Bounds on Light Scalar Particles, *Phys. Lett. B* **228**, 264 (1989).
- [36] L. Amendola, Scaling solutions in general nonminimal coupling theories, *Phys. Rev. D* **60**, 043501 (1999), [arXiv:astro-ph/9904120](#).
- [37] G. R. Farrar and P. J. E. Peebles, Interacting dark matter and dark energy, *Astrophys. J.* **604**, 1 (2004), [arXiv:astro-ph/0307316](#).
- [38] W. Zimdahl and D. Pavon, Statefinder parameters for interacting dark energy, *Gen. Rel. Grav.* **36**, 1483 (2004), [arXiv:gr-qc/0311067](#).
- [39] H. M. Sadjadi and M. Alimohammadi, Cosmological coincidence problem in interactive dark energy models, *Phys. Rev. D* **74**, 103007 (2006), [arXiv:gr-qc/0610080](#).
- [40] S. Hussain, S. Chakraborty, N. Roy, and K. Bhattacharya, Dynamical systems analysis of tachyon-dark-energy models from a new perspective, *Phys. Rev. D* **107**, 063515 (2023), [arXiv:2208.10352 \[gr-qc\]](#).
- [41] S. Das, S. Hussain, D. Nandi, R. O. Ramos, and R. Silva, Stability analysis of warm quintessential dark energy model, *Phys. Rev. D* **108**, 083517 (2023), [arXiv:2306.09369 \[gr-qc\]](#).
- [42] L. Amendola, Coupled quintessence, *Phys. Rev. D* **62**, 043511 (2000), [arXiv:astro-ph/9908023](#).
- [43] A. Nunes, J. P. Mimoso, and T. C. Charters, Scaling solutions from interacting fluids, *Phys. Rev. D* **63**, 083506 (2001), [arXiv:gr-qc/0011073](#).
- [44] L. P. Chimento, A. S. Jakubi, D. Pavon, and W. Zimdahl, Interacting quintessence solution to the coincidence problem, *Phys. Rev. D* **67**, 083513 (2003), [arXiv:astro-ph/0303145](#).
- [45] X. Zhang, Coupled quintessence in a power-law case and the cosmic coincidence problem, *Mod. Phys. Lett. A* **20**, 2575 (2005), [arXiv:astro-ph/0503072](#).
- [46] C. G. Boehmer, G. Caldera-Cabral, R. Lazkoz, and R. Maartens, Dynamics of dark energy with a coupling to dark matter, *Phys. Rev. D* **78**, 023505 (2008), [arXiv:0801.1565 \[gr-qc\]](#).
- [47] M. Baldi, V. Pettorino, G. Robbers, and V. Springel, Hydrodynamical N-body simulations of coupled dark energy cosmologies, *Mon. Not. Roy. Astron. Soc.* **403**, 1684 (2010), [arXiv:0812.3901 \[astro-ph\]](#).
- [48] G. Leon and E. N. Saridakis, Phantom dark energy with varying-mass dark matter particles: acceleration and cosmic coincidence problem, *Phys. Lett. B* **693**, 1 (2010), [arXiv:0904.1577 \[gr-qc\]](#).
- [49] E. Majerotto, J. Valiviita, and R. Maartens, Adiabatic initial conditions for perturbations in interacting dark energy models, *Mon. Not. Roy. Astron. Soc.* **402**, 2344 (2010), [arXiv:0907.4981 \[astro-ph.CO\]](#).
- [50] J. Valiviita, R. Maartens, and E. Majerotto, Observational constraints on an interacting dark energy model, *Mon. Not. Roy. Astron. Soc.* **402**, 2355 (2010), [arXiv:0907.4987 \[astro-ph.CO\]](#).
- [51] M. Cataldo, F. Arevalo, and P. Minning, On a class of scaling FRW cosmological models, *JCAP* **02**, 024, [arXiv:1002.3415 \[astro-ph.CO\]](#).
- [52] M. Baldi, Time dependent couplings in the dark sector: from background evolution to nonlinear structure formation, *Mon. Not. Roy. Astron. Soc.* **411**, 1077 (2011), [arXiv:1005.2188 \[astro-ph.CO\]](#).
- [53] G. Leon, P. Silveira, and C. R. Fadrugas, Phase-space of flat Friedmann-Robertson-Walker models with both a scalar field coupled to matter and radiation, (2010), [arXiv:1009.0689 \[gr-qc\]](#).
- [54] T. Clemson, K. Koyama, G.-B. Zhao, R. Maartens, and J. Valiviita, Interacting Dark Energy – constraints and degeneracies, *Phys. Rev. D* **85**, 043007 (2012), [arXiv:1109.6234 \[astro-ph.CO\]](#).
- [55] C. R. Fadrugas and G. Leon, Some remarks about non-minimally coupled scalar field models, *Class.*

- Quant. Grav.* **31**, 195011 (2014), [arXiv:1405.2465 \[gr-qc\]](#).
- [56] S. Pan, W. Yang, C. Singha, and E. N. Saridakis, Observational constraints on sign-changeable interaction models and alleviation of the  $H_0$  tension, *Phys. Rev. D* **100**, 083539 (2019), [arXiv:1903.10969 \[astro-ph.CO\]](#).
- [57] S. Gariazzo, E. Di Valentino, O. Mena, and R. C. Nunes, Late-time interacting cosmologies and the Hubble constant tension, *Phys. Rev. D* **106**, 023530 (2022), [arXiv:2111.03152 \[astro-ph.CO\]](#).
- [58] S. Sen and A. A. Sen, Late time acceleration in Brans-Dicke cosmology, *Phys. Rev. D* **63**, 124006 (2001), [arXiv:gr-qc/0010092](#).
- [59] S. Nojiri, S. D. Odintsov, and M. Sasaki, Gauss-Bonnet dark energy, *Phys. Rev. D* **71**, 123509 (2005), [arXiv:hep-th/0504052](#).
- [60] O. Bertolami, F. S. N. Lobo, and J. Paramos, Non-minimum coupling of perfect fluids to curvature, *Phys. Rev. D* **78**, 064036 (2008), [arXiv:0806.4434 \[gr-qc\]](#).
- [61] O. Bertolami and A. Martins, On the dynamics of perfect fluids in non-minimally coupled gravity, *Phys. Rev. D* **85**, 024012 (2012), [arXiv:1110.2379 \[gr-qc\]](#).
- [62] S. Tsujikawa and M. Sami, String-inspired cosmology: Late time transition from scaling matter era to dark energy universe caused by a Gauss-Bonnet coupling, *JCAP* **01**, 006, [arXiv:hep-th/0608178](#).
- [63] D. Bettoni and S. Liberati, Dynamics of non-minimally coupled perfect fluids, *JCAP* **08**, 023, [arXiv:1502.06613 \[gr-qc\]](#).
- [64] A. Chatterjee, S. Hussain, and K. Bhattacharya, Dynamical stability of the k-essence field interacting nonminimally with a perfect fluid, *Phys. Rev. D* **104**, 103505 (2021), [arXiv:2105.00361 \[gr-qc\]](#).
- [65] K. Bhattacharya, A. Chatterjee, and S. Hussain, Dynamical stability in presence of non-minimal derivative dependent coupling of k-essence field with a relativistic fluid, *Eur. Phys. J. C* **83**, 488 (2023), [arXiv:2206.12398 \[gr-qc\]](#).
- [66] T. S. Koivisto, E. N. Saridakis, and N. Tamanini, Scalar-Fluid theories: cosmological perturbations and large-scale structure, *JCAP* **09**, 047, [arXiv:1505.07556 \[astro-ph.CO\]](#).
- [67] S. Hussain, A. Chatterjee, and K. Bhattacharya, Dynamical stability in models where dark matter and dark energy are nonminimally coupled to curvature, *Phys. Rev. D* **108**, 103502 (2023), [arXiv:2305.19062 \[gr-qc\]](#).
- [68] G. Leon, On the Past Asymptotic Dynamics of Non-minimally Coupled Dark Energy, *Class. Quant. Grav.* **26**, 035008 (2009), [arXiv:0812.1013 \[gr-qc\]](#).
- [69] C. G. Boehmer, N. Tamanini, and M. Wright, Interacting quintessence from a variational approach Part I: algebraic couplings, *Phys. Rev. D* **91**, 123002 (2015), [arXiv:1501.06540 \[gr-qc\]](#).
- [70] C. G. Boehmer, N. Tamanini, and M. Wright, Interacting quintessence from a variational approach Part II: derivative couplings, *Phys. Rev. D* **91**, 123003 (2015), [arXiv:1502.04030 \[gr-qc\]](#).
- [71] N. Tamanini, Phenomenological models of dark energy interacting with dark matter, *Phys. Rev. D* **92**, 043524 (2015), [arXiv:1504.07397 \[gr-qc\]](#).
- [72] R. Kase and S. Tsujikawa, Scalar-Field Dark Energy Nonminimally and Kinetically Coupled to Dark Matter, *Phys. Rev. D* **101**, 063511 (2020), [arXiv:1910.02699 \[gr-qc\]](#).
- [73] J. D. Brown, Action functionals for relativistic perfect fluids, *Class. Quant. Grav.* **10**, 1579 (1993), [arXiv:gr-qc/9304026](#).
- [74] J. Valiviita, E. Majerotto, and R. Maartens, Instability in interacting dark energy and dark matter fluids, *JCAP* **07**, 020, [arXiv:0804.0232 \[astro-ph\]](#).
- [75] L. H. Ford, Gravitational Particle Creation and Inflation, *Phys. Rev. D* **35**, 2955 (1987).
- [76] I. Prigogine, J. Gehehiau, E. Gunzig, and P. Nardone, Thermodynamics of cosmological matter creation, *Proc. Nat. Acad. Sci.* **85**, 7428 (1988).
- [77] W. Zimdahl and D. Pavon, Cosmology with adiabatic matter creation, *Int. J. Mod. Phys. D* **3**, 327

- (1994).
- [78] W. Zimdahl and D. Pavon, Fluid cosmology with decay and production of particles, *Gen. Rel. Grav.* **26**, 1259 (1994).
- [79] W. Zimdahl, Bulk viscous cosmology, *Phys. Rev. D* **53**, 5483 (1996), [arXiv:astro-ph/9601189](#).
- [80] R. C. Nunes and S. Pan, Cosmological consequences of an adiabatic matter creation process, *Mon. Not. Roy. Astron. Soc.* **459**, 673 (2016), [arXiv:1603.02573 \[gr-qc\]](#).
- [81] W. Zimdahl, Cosmological particle production and generalized thermodynamic equilibrium, *Phys. Rev. D* **57**, 2245 (1998), [arXiv:gr-qc/9711081](#).
- [82] W. Zimdahl, Cosmological particle production, causal thermodynamics, and inflationary expansion, *Phys. Rev. D* **61**, 083511 (2000), [arXiv:astro-ph/9910483](#).
- [83] K. Bhattacharya, A. Chatterjee, and S. Hussain, The nature of cosmological metric perturbations in presence of gravitational particle production, *Gen. Rel. Grav.* **54**, 84 (2022), [arXiv:2007.00904 \[gr-qc\]](#).
- [84] W. Zimdahl and D. Pavón, Reheating and adiabatic particle production, *Monthly Notices of the Royal Astronomical Society* **266**, 872 (1994), <https://academic.oup.com/mnras/article-pdf/266/4/872/3051080/mnras266-0872.pdf>.
- [85] J. A. S. Lima, S. Basilakos, and F. E. M. Costa, New Cosmic Accelerating Scenario without Dark Energy, *Phys. Rev. D* **86**, 103534 (2012), [arXiv:1205.0868 \[astro-ph.CO\]](#).
- [86] V. H. Cárdenas, M. Cruz, S. Lepe, S. Nojiri, and S. D. Odintsov, Challenging matter creation models in the phantom divide, *Phys. Rev. D* **101**, 083530 (2020), [arXiv:2004.02337 \[gr-qc\]](#).
- [87] A. D. Rendall, Cosmological models and center manifold theory, *Gen. Rel. Grav.* **34**, 1277 (2002), [arXiv:gr-qc/0112040](#).
- [88] S. Bahamonde, C. G. Böhm, S. Carloni, E. J. Copeland, W. Fang, and N. Tamanini, Dynamical systems applied to cosmology: dark energy and modified gravity, *Phys. Rept.* **775-777**, 1 (2018), [arXiv:1712.03107 \[gr-qc\]](#).
- [89] J. Dutta, W. Khylllep, and N. Tamanini, Dark energy with a gradient coupling to the dark matter fluid: cosmological dynamics and structure formation, *JCAP* **01**, 038, [arXiv:1707.09246 \[gr-qc\]](#).
- [90] A. A. Coley, *Dynamical systems and cosmology* (Kluwer, Dordrecht, Netherlands, 2003).
- [91] U. Elias and H. Gingold, Critical points at infinity and blow up of solutions of autonomous polynomial differential systems via compactification, *Journal of mathematical analysis and applications* **318**, 305 (2006).
- [92] R. I. Ivanov and E. M. Prodanov, On the Cosmological Models with Matter Creation, *Eur. Phys. J. C* **79**, 973 (2019), [arXiv:1911.04380 \[gr-qc\]](#).
- [93] U. Elias and H. Gingold, Critical points at infinity and blow up of solutions of autonomous polynomial differential systems via compactification, *Journal of Mathematical Analysis and Applications* **318**, 305 (2006).
- [94] S. Hussain, S. Nelleri, and K. Bhattacharya, Comparative Analysis of  $k$ -essence and Quintessence Scalar Field Models: A Data Analysis Approach, (2024), [arXiv:2406.07179 \[astro-ph.CO\]](#).
- [95] S. Cao, T.-J. Zhang, X. Wang, and T. Zhang, Cosmological Constraints on the Coupling Model from Observational Hubble Parameter and Baryon Acoustic Oscillation Measurements, *Universe* **7**, 57 (2021), [arXiv:2103.03670 \[astro-ph.CO\]](#).
- [96] L. Perivolaropoulos and F. Skara, On the homogeneity of SnIa absolute magnitude in the Pantheon+ sample, *Mon. Not. Roy. Astron. Soc.* **520**, 5110 (2023), [arXiv:2301.01024 \[astro-ph.CO\]](#).
- [97] D. Brout *et al.*, The Pantheon+ Analysis: Cosmological Constraints, *Astrophys. J.* **938**, 110 (2022), [arXiv:2202.04077 \[astro-ph.CO\]](#).
- [98] H. Amirhashchi and S. Amirhashchi, Constraining Bianchi Type I Universe With Type Ia Supernova



- and  $H(z)$  Data, *Phys. Dark Univ.* **29**, 100557 (2020), [arXiv:1802.04251 \[astro-ph.CO\]](https://arxiv.org/abs/1802.04251).
- [99] J. Skilling, Nested Sampling, *AIP Conference Proceedings* **735**, 395 (2004).
- [100] J. Skilling, Nested sampling for general bayesian computation, *Bayesian Analysis* , 833 (2006).
- [101] J. S. Speagle, dynesty: a dynamic nested sampling package for estimating bayesian posteriors and evidences, *Monthly Notices of the Royal Astronomical Society* **493**, 3132–3158 (2020).
- [102] E. Higson, W. Handley, M. Hobson, and A. Lasenby, Dynamic nested sampling: an improved algorithm for parameter estimation and evidence calculation, *Statistics and Computing* **29**, 891–913 (2018).
- [103] A. Lewis, *Getdist: a python package for analysing monte carlo samples* (2019), [arXiv:1910.13970 \[astro-ph.IM\]](https://arxiv.org/abs/1910.13970).
- [104] R. Trotta, Bayes in the sky: Bayesian inference and model selection in cosmology, *Contemp. Phys.* **49**, 71 (2008), [arXiv:0803.4089 \[astro-ph\]](https://arxiv.org/abs/0803.4089).
- [105] A. de la Cruz-Dombriz, P. K. S. Dunsby, O. Luongo, and L. Reverberi, Model-independent limits and constraints on extended theories of gravity from cosmic reconstruction techniques, *JCAP* **12**, 042, [arXiv:1608.03746 \[gr-qc\]](https://arxiv.org/abs/1608.03746).
- [106] K. P. Burnham and D. R. Anderson, Multimodel inference: Understanding aic and bic in model selection, *Sociological Methods & Research* **33**, 261 (2004), <https://doi.org/10.1177/0049124104268644>.
- [107] J. Shi, Cosmological constraints in covariant  $f(Q)$  gravity with different connections, *Eur. Phys. J. C* **83**, 951 (2023), [arXiv:2307.08103 \[gr-qc\]](https://arxiv.org/abs/2307.08103).